https://doi.org/10.5194/essd-2024-596
Preprint. Discussion started: 14 January 2025

Open Access Earth System Science Data Discussions

Large-scale forest stand height mapping in the northeastern U.S. and China using L-band spaceborne repeat-pass InSAR and GEDI LiDAR data

Yanghai Yu[1], Yang Lei[1], Paul Siqueira[2], Xiaotong Liu[3], Denuo Gu[4], Anmin Fu[3], Yong Pang[4], Wenli Huang[5], Jiancheng Shi[1]

[1]National Space Science Center, Chinese Academy of Sciences, Beijing, 100190, China
[2]Department of Electrical and Computer Engineering, University of Massachusetts, Amherst, MA 01003-9284, USA
[3]Academy of Forest Inventory and Planning, State Forestry Administration, Beijing 100714, China
[4]Institute of Forest Resource Information Techniques, Chinese Academy of Forestry, Beijing 100091, China
[5] School of Resource and Environmental Science, Wuhan University, Wuhan 430079, China

Correspondence to: Yang Lei (leiyang@nssc.ac.cn)

Abstract. This paper presents a global-to-local fusion approach combining spaceborne Synthetic Aperture Radar (SAR) Interferometry (InSAR) and LiDAR to create large-scale mosaics of forest stand height. The forest height estimates are derived based on a semi-empirical InSAR scattering model, which links the forest height to repeat-pass InSAR coherence magnitudes. The sparsely yet extensively distributed LiDAR samples provided by Global Ecosystem Dynamics Investigation (GEDI) mission enable the parametrization of signal model at a finer spatial scale. The proposed global-to-local fitting strategy allows for efficient use of LiDAR samples to determine adaptive model at reginal scale, leading to improved forest height estimates by integrating InSAR-LiDAR under nearly concurrent acquisition condition. This is supported by fusing the ALOS-2 and GEDI data at several representative forest sites. This approach is further applied to the open-access ALOS InSAR data to evaluate its large-scale mapping capabilities. To address temporal mismatch between the GEDI and ALOS acquisitions, the forest disturbances or deforestation areas are first identified by integrating ALOS-2 backscatter products and GEDI data. Further, a modified signal model is developed and analysed accounting for natural forest growth over temperate forest regions where the intact forest landscape along with forest height remain quite stable and only change slightly as trees grow. In the absence of detailed statistical data on forest growth, the modified signal model can be well approximated using the original model at regional scale via local fitting. To validate this, two forest height mosaic maps based on ALOS-1 data were generated for the entire northeastern regions of U.S. and China with total area of 18 million and 152 million hectares, respectively. The validation of the forest height estimates demonstrates improved accuracy achieved by the proposed approach compared to the previous efforts i.e., reducing from a 4 m RMSE on the order of 3-6-ha aggregated pixel size to 3.8 m RMSE at 0.8-ha pixel size. This updated fusion approach not only fills in the sparse spatial sampling of individual GEDI footprints, but also improves the accuracy of forest height estimates by 20% compared to the interpolated GEDI maps. Extensive evaluation of forest height inversion against LVIS LiDAR data indicates an accuracy 3-4 m over flat

https://doi.org/10.5194/essd-2024-596
Preprint. Discussion started: 14 January 2025

Open Access Earth System Science Data Discussions

areas and 4-5 m over hilly areas in the New England region, whereas the forest height estimates over the northeastern China are best compared with small footprint LiDAR validation data even at an accuracy of below 3.5 m and with a coefficient of determination, R^2, mostly above 0.6. Given the achieved accuracy for forest height estimates, this fusion prototype offers as a cost-effective solution for public users to obtain wall-to-wall forest height maps at large scale using freely accessible spaceborne repeat-pass L-band InSAR (e.g. forthcoming NISAR) and LiDAR (e.g. GEDI) data.

1 Introduction

Forests play a crucial role in the terrestrial ecosystem as they serve as one of the largest terrestrial carbon pool (Pan et al., 2011). As identified by IPCC v6 (Masson-Delmotte et al., 2021) and international forest monitoring efforts such as United Nation's REDD+ programme (Angelsen, 2009), large-scale (e.g., state, continental, and global) forest height products are desired to quantify carbon storage in forested resources due to their close relationship to aboveground biomass (AGB). These products also help to determine forests' roles in climate change mitigation and biodiversity conservation (Houghton, Hall et al. 2009). In this work, "forest height" or "forest stand height" (FSH) are referred to as the large footprint (25 m) LiDAR-determined relative height at the 98th percentile (rh98) as measured by NASA' GEDI LiDAR mission onboard the International Space Station (ISS).

Satellite-based remote sensing represents a cost-effective method to investigate biophysical parameters of forests. Commonly used remote sensing methods include optical and microwave imaging observations, such as passive optical sensors including Landsat series (Loveland and Dwyer, 2012), LiDAR including ICESat-1/2 (Schutz et al., 2005; Abdalati et al., 2010) and GEDI (Dubayah et al., 2020) missions, and SAR systems such as JAXA's ALOS/ALOS-2 (Rosenqvist et al., 2007; Rosenqvist et al., 2014), Sentinel-1 (Torres et al., 2012), TanDEM-X (Krieger et al., 2007). LiDAR and SAR are promising to capturing the internal vertical structure of forests: LiDAR is fundamentally sensitive to structure, while radar is sensitive to the sensitive to the three-dimensional distribution of vegetation elements (Ulaby et al., 1990). The backscatter information from a single SAR imagery can be used for inferring the above-ground biomass (Santoro et al., 2021), despite the fact that the actual vertical information remains undetermined. As an extension of SAR backscatter observation, SAR interferometry provide direct information related to the vertical forest structure (Treuhaft and Siqueira, 2000). Spaceborne InSAR can operate either by single-pass interferometric measurements in a bistatic configuration (e.g., TanDEM-X missions (Krieger et al., 2007)), or by repeat-pass InSAR (e.g. ALOS-1/2 L-band, Sentinel-1 C-band missions). The short wavelength operated in former satellites may restrict its sensing capabilities over dense forests, while temporal decorrelation affects repeat-pass InSAR performance (Zebker and Villasenor, 1992; Monti-Guarnieri et al., 2020; Lavalle et al., 2012; Ahmed et al., 2011). LiDAR has been widely used for characterizing the forest vertical structure at regional scale, and can also be considered as the reference for calibrating and validating other forest height inversion models as well as radar-derived forest height estimates (Choi et al., 2023; Askne et al., 2013). Spaceborne LiDAR (Schutz et al., 2005) have been further developed

https://doi.org/10.5194/essd-2024-596
Preprint. Discussion started: 14 January 2025

for globally monitoring of ecosystems. Because of observational constraints, these measurements have been based on such a spatial sampling technique that only sparsely yet extensively distributed measurements can be collected.

For instance, the NASA's GEDI mission (Dubayah et al., 2020a) is the first spaceborne LiDAR instrument designed to study ecosystems. Since 2019, GEDI has provided extensively distributed LiDAR waveform measurements for the nearly global forests. These waveform observations allow for the extraction of various biophysical parameters, such as canopy height and canopy leaf area index. However, GEDI collects only discrete point measurements, spaced approximately 60 meters apart in the along-track direction and 600 meters apart in the cross-track direction. To overcome this limitation and extend GEDI's measurements into continuous datasets, several fusion studies have been conducted. Notable examples include efforts that incorporate radiometric information from optical sensors, such as NASA's Landsat (Potapov et al., 2021) and ESA's Sentinel-2 (Lang et al., 2022), as well as from SAR backscatter signals (Shendryk, 2022). However, relying solely on radiometric information to expand LiDAR observations has proven suboptimal, particularly in high-biomass regions where signal saturation occurs (Kalacska et al., 2007, Imhoff, 1995, Ho Tong Minh et al., 2016).

In contrast, because of its fundamental sensitivity to height and/or variations in height, the fusion of SAR interferometry and GEDI has gained much interests. For example, making joint use of TanDEM-X and GEDI data has been assessed and demonstrated for achieving wall-to-wall forest height and AGB mapping (Qi and Dubayah, 2016, Choi et al., 2023, Guliaev et al., 2021, Qi et al., 2019). Without the effects of temporal decorrelation, the forest height was inverted in these studies based on the Random Volume Over Ground (RVoG) model (Treuhaft and Siqueira, 2000, Cloude and Papathanassiou, 1998) and an external constraint induced by GEDI waveform information. That is, only the mean waveform information across the scene in these studies was used for model-based inversion, implying an underlying assumption that the forest objects over the scene share a similar vertical structure. This may lead to a degraded performance when dealing with spatially heterogenous forests. Additionally, a potential limitation of TanDEM-X observations is the insufficient penetration capability over dense forests due to the short wavelength of the X-band (~0.01 m) (Kugler et al., 2014).

An alternative to these approaches is to use the temporal decorrelation itself (Lei et al., 2017) with negligible spatial baselines. This method was initially demonstrated by using a relatively small strip of airborne LiDAR data as the reference to create a forest height mosaic over a two-state region in the northeastern U.S. (Lei et al., 2018). Given the limited availability of LiDAR datasets at that time, scene-wide constant model parameters for the relationship between the InSAR temporal decorrelation and LiDAR observations were assumed and the overlapping area between InSAR scenes were used to propagate the LiDAR information throughout the adjacent InSAR scenes. With the successful launch of the GEDI, the introduction of local GEDI samples into the model inversion was achieved in a preliminary effort (Lei and Siqueira, 2022).

https://doi.org/10.5194/essd-2024-596
Preprint. Discussion started: 14 January 2025

Open Access Earth System Science Data Discussions

This paper further removes the assumption of spatially constant temporal change model that were made in the previous efforts, and develops a new inversion approach based on a two-stage (global-to-local) inversion algorithm. By efficiently leveraging regional GEDI samples, this approach enables finer-scale characterization of temporal decorrelation patterns, resulting in much improved accuracy in forest height inversion. This approach is validated by fusing ALOS-2 InSAR and GEDI data acquired under nearly concurrent conditions. Furthermore, the approach is applied to the open-access ALOS InSAR data for evaluating its large-scale mapping capability. To address the temporal mismatch between the ALOS and GEDI acquisition, forest disturbance can be detected by fusing SAR backscatter and LiDAR data under nearly concurrent condition. Furthermore, a modified model is developed to account for the natural growth of forests over temperate forest regions where the Intact Forest Landscape (IFL) exhibit slow changes in height. Without available forest growth data, the modified signal model can be well approximated using the original signal model at regional scale through local fitting. Two 30 m gridded forest height mosaics were generated for the northeastern regions of U.S. and China. Validation of the generated forest height mosaics against extensive airborne LiDAR observations demonstrate enhanced inversion accuracy at sub-hectare pixel size. The key contribution of this paper lies in the efficient use of local GEDI information for radar-LiDAR data fusion, enabling more accurate forest height estimates using open-access spaceborne data, such as GEDI and forthcoming NiSAR (Siqueira et al., 2024; Kellogg et al., 2020) data.

This paper is structured as follows: Section 2 reviews the theoretical background, followed by the proposed methodology. Section 3 introduces the study area and available experimental datasets. Section 4 validates the forest height estimates over a variety of forest sites in the northeastern U.S. and China. Conclusions and discussion are provided in Section 5.

2 Signal model and inversion

After standard InSAR preprocessing (including coregistration, and topographic phase compensation, etc), a complex InSAR correlation observation between two SAR images can be derived by:

$$\gamma = \frac{\langle I_1 \cdot I_2^* \rangle_L}{\sqrt{\langle I_1 \cdot I_1^* \rangle_L \langle I_2 \cdot I_2^* \rangle_L}} \tag{1}$$

where I_1 and I_2 represent two SAR images from the 1st and 2nd acquisition, respectively, the operator $\langle \cdot \rangle_L$ is used for spatial averaging of L looks, As a metric to measure similarity, the complex InSAR correlation accounts for various forms of decorrelation (Zebker and Villasenor, 1992; Gatelli et al., 1994; Treuhaft and Siqueira, 2000). If we consider a pair of SAR images with short spatial separation over forested area, InSAR coherence can be expressed as:

$$|\gamma| = |\gamma_{SNR}| \cdot |\gamma_{geo}| \cdot |\gamma_{v\&t}| \tag{2}$$

where γ_{SNR} represents the decorrelation induced by the radar-return signal to noise ratio, and γ_{geo} denotes the geometric decorrelation due to the difference between two look angles. After accounting for SNR decorrelation and performing common band filtering (Gatelli et al., 1994), the remaining component of correlation, $\gamma_{v\&t}$, is only related to temporal

https://doi.org/10.5194/essd-2024-596
Preprint. Discussion started: 14 January 2025

changes and the distribution of scatterers in the vertical direction. The spatial separation for one InSAR pair is usually indicated by the interferometric vertical wavenumber κ_z (unit rad/m)(Bamler and Hartl, 1998). A small value of κ_z (less than 0.05 rad/m) is usually suggested by the analysis in (Lei and Siqueira, 2014).

For moderate and large temporal baselines, moisture-induced dielectric fluctuations and wind-induced random motion are identified as the primary factors influencing temporal decorrelation (Lavalle et al., 2012; Askne et al., 1997). (Lei et al., 2017) introduced a modified Random Volume over Ground (RVoG) model that accounts for the coupled effects of dielectric changes and random motion in spaceborne ALOS observations. The model is further simplified by assuming negligible ground scattering under cross-polarized (HV) observations and short spatial baselines, and establishes a semi-empirical formula linking cross-polarized InSAR coherence magnitude ($\gamma_{v\&t}^{HV}$) to forest height (h_v):

$$|\gamma_{v\&t}^{HV}| = S \cdot \text{sinc}\left(\frac{h_v}{C}\right), \text{with } 0 \le h_v \le \pi C \quad \textbf{(3)}$$

where S (ranging from 0 to 1; unitless) is a parameter primarily connected to moisture-induced dielectric changes in the target, and C (a positive value that has units of meters) relates to the wind-induced random motion. In practice, ground scattering remains present in cross-polarized signals, particularly for low-frequency SAR observations. However, it is typically minimal, with a ground-to-volume ratio generally less than 0.1. This residual ground scattering can bias forest height estimates, particularly for short or very tall forest stands. It is also important to note that this formula is valid when the interferometric vertical wavenumber is below 0.15 rad/m and is most reliable when smaller than 0.05 rad/m (Lei and Siqueira, 2014), which is consistent with the acquisition geometry of ALOS1-2 InSAR acquisition. Otherwise, the presence of volumetric decorrelation will result in a compromised inversion performance.

2.1 Fusing concurrent radar-lidar acuqisitions by a global-to-local inversion approach

Determination of the above temporal decorrelation model (3) has to resort to ancillary forest height data e.g., field inventory data, LiDAR measurements, and etc. A global-to-local procedure is used for determination, since the regional forests are usually relatively homogenous, leading to the construction of ill-conditioned observations for model determination. A global initial guess is firstly needed for constraining the solution space for subsequent fitting.

For one InSAR scene, a constant scene-wide behavior of the temporal change parameters is firstly assumed, e.g., (S_{scene}, C_{scene}). To one candidate pair of these parameters, forest height estimates $\widehat{h_v}$ are derived by solving the model (3) based on InSAR coherence magnitude. A covariance matrix between $\widehat{h_v}$ and the ancillary forest height h_a from LiDAR and its eigen-decomposition are expressed by:

$$\Sigma = \begin{bmatrix} \text{cov}(\widehat{h_v}, \widehat{h_v}) & \text{cov}(\widehat{h_v}, h_a) \\ \text{cov}(\widehat{h_v}, h_a) & \text{cov}(h_a, h_a) \end{bmatrix} = Q\Lambda Q^{-1} \quad \textbf{(4)}$$

https://doi.org/10.5194/essd-2024-596
Preprint. Discussion started: 14 January 2025

where the 2×2 matrix Q contains the eigen vectors, the 2×2 diagonal matrix Λ comprises the eigen values. The function $\mathrm{cov}(A, B)$ denotes the covariance between the two vectors A and B:

$$\mathrm{cov}(A, B) = \frac{1}{N-1}\sum_{i=1}^{N}(A-\mu_A)\cdot(B-\mu_B) \tag{5}$$

with μ_A and μ_B being the mean values of two input vectors. Two fitting metrics e.g., slope k and bias b can be extracted out of the constructed covariance matrix:

$$k = \frac{Q_{21}}{Q_{11}} \tag{6}$$

$$b = 2\frac{\mu_{\widehat{h_v}} - \mu_{\mathrm{h}_a}}{\mu_{\widehat{h_v}} + \mu_{\mathrm{h}_a}} \tag{7}$$

By defining a figure of merit i.e. approaching zero bias and unity slope (i.e. the 1:1 line), a pair of temporal parameters are determined by minimizing the objective function:

$$\{S_{scene}, C_{scene}\} = \arg\min_{S,C}(b^2 + (k-1)^2) \tag{8}$$

Resolving model parameters (S_{scene}, C_{scene}) is referred to as global fitting strategy. The effectiveness of this approach was demonstrated over the northeastern U.S. (Lei et al., 2018) if well-constructed observation vectors including sufficient samples ranging from low trees to tall trees[1].

Because temporal change factors tend to be spacing-varying with respect to vegetation types and weather/climate conditions, inversion performance for solely global fitting as described above is expected to deteriorate when applied for large-scale inversion. With the availability of GEDI data, a substantial improvement is expected by expressing decorrelation model at a finer spatial scale. An preliminary effort was made in (Lei and Siqueira, 2022) where the determination of (S, C) is carried out on each GEDI LiDAR sample $h_{gedi}(i, j)$ to obtain $S(i, j)$ and $C(i, j)$, where i and j represent latitude and longitude for each GEDI sample. As only one sample cannot provide sufficient observations to resolve two unknowns so that an external constraint on the ratio of $S(i, j)/C(i, j)$ was introduced.

Each individual GEDI measurement is subject to errors caused by artifacts such as terrain slopes (Wang et al., 2019) and systematic geo-location inaccuracies (ranging from several meters to tens of meters) (Tang et al., 2023). Additionally, the penetration of the LiDAR signal is sometimes limited within GEDI's coverage beams (Dubayah et al., 2020b). InSAR coherence estimates also experience measurement uncertainty (Rodriguez and Martin, 1992; Touzi et al., 1999). To address these challenges, spatial averaging is commonly used to reduce errors for both coherence and GEDI measurements.

[1] This fitting metric has proven to be more robust than the Euclidean norm for a data cloud with large measurement uncertainty (Lei and Siqueira, 2014).

https://doi.org/10.5194/essd-2024-596
Preprint. Discussion started: 14 January 2025

In this context, a local fitting step is introduced to acquire temporal change factors at a finer spatial scale using extensive GEDI information: a circular window (32 pixels, 960 m wide) is set for each GEDI sample to collect regional samples and their corresponding InSAR coherence magnitude observations. A Euclidean norm-based fitting is used since a local window tends to encompass homogeneous vegetation with similar heights so that the global k-b fitting metric is no longer robust. Assuming consistent temporal change factors within each local window, the factors can be determined by:

$$\{S(i,j), C(i,j)\} = \arg\min_{S,C} \sum_{(r,c)\epsilon W} \left(\widehat{h_v}(i+r, j+c) - h_{gedi}(i+r, j+c)\right)^2 \tag{9}$$

where W is the local searching window in geographic coordinate system with r and c being local indices along the latitude and longitude direction within the local window. To preserve detailed information, weighting factors based on distance or similarity metric are used in local fitting, as in:

$$\{S(i,j), C(i,j)\} = \arg\min_{S,C} \frac{\sum_{(r,c)\epsilon W} \left[w(r,c)\left(\widehat{h_v}(i+r, j+c) - h_{gedi}(i+r, j+c)\right)\right]^2}{\sum_{(r,c)\epsilon W} w(r,c)^2} \tag{10}$$

where the weights can be set based on spatial distances between neighboring pixels and the central pixel within the local window, or adapted depending on land-cover type (Deledalle et al., 2014). For simplicity and versatility, the spatial distance-based weight setting, as exemplified in Figure 1, has been used for inversion in this work. As the parameters were determined on the grid of GEDI samples, a post-interpolation is needed to obtain gridded temporal parameters for matching the InSAR scene.

It should be noted that this physical scattering model (3) is established for forested areas, meaning it does not adequately address other land-cover types, such as water bodies and urban areas. Furthermore, actively managed regions (e.g., cropland) are subject to additional decorrelation effects induced by human activities. It was suggested to use L-band backscatter-based height estimates to improve the inversion in these instances. The backscatter-based inversion are derived based on an exponential model (Yu and Saatchi, 2016; Lucas et al., 2006) which can be determined using the similar global-to-local routine as the proposed approach. In practice, only global fitting strategy is used for model parametrization as it provides accurate estimates as compared to global-to-local fitting (slightly worse) while maintains an affordable computational expense. After that, the estimates of active land management areas in coherence-based inversion are replaced by the corresponding backscatter-based estimates.

https://doi.org/10.5194/essd-2024-596
Preprint. Discussion started: 14 January 2025

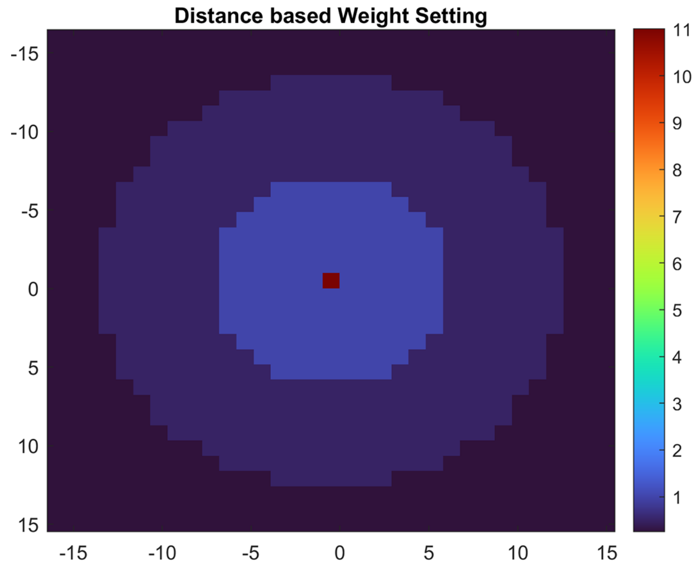

Figure 1: An illustrated example of distance-based weight setting for a 0.96 km (32 by 32 pixels) wide moving boxcar window. The selection of window size is a compromise between smooth and detailed information. This window size is selected here for including enough samples for model fitting while maintaining local homogenous.

2.2 Fusing non-concurrent radar-lidar data

2.2.1 Addressing Forest disturbance or Deforestation

The acquisition times between repeat-pass InSAR and spaceborne LiDAR usually do not overlap in practice. For example, the ALOS-2 InSAR acquisitions would match those of GEDI ideally; however, there are not many ALOS-2 InSAR pairs available in the data archive that is freely accessible. In contrast, ALOS InSAR pairs are consistently available covering the study regions; however, there is an approximate 10-year time gap. To address this issue, a two-fold solution is provided in the following sections. The temporal evolution of forests is primarily influenced by two factors: forest disturbance (including deforestation) and natural growth. Forest disturbance or deforestation leads to forest loss and, in some cases, conversion to other land uses, such as bare ground. This change is poorly characterized by the signal model and must be addressed in advance.

The height of bare ground and short vegetation ($\leq 10\,m$) is better inverted by jointly using the SAR backscatter and spaceborne LiDAR information with respect to the inversion based on the InSAR correlation (Lei, 2016). Moreover, annual global backscatter products are available from the archive of JAXA, enabling the fusion of the ALOS-2 SAR backscatter information and spaceborne LiDAR under nearly concurrent acquisition conditions. Figure 2 presents an example of how the forest loss is detected by SAR backscatter-based inversion within the New England region: the majority of forest disturbance

https://doi.org/10.5194/essd-2024-596
Preprint. Discussion started: 14 January 2025

areas as defined by the global forest change products (Hansen et al., 2013) were detected by the backscatter-based estimates. Based on the statistics over the New England region, 72% of disturbed areas have been detected using the backscatter-based estimates.

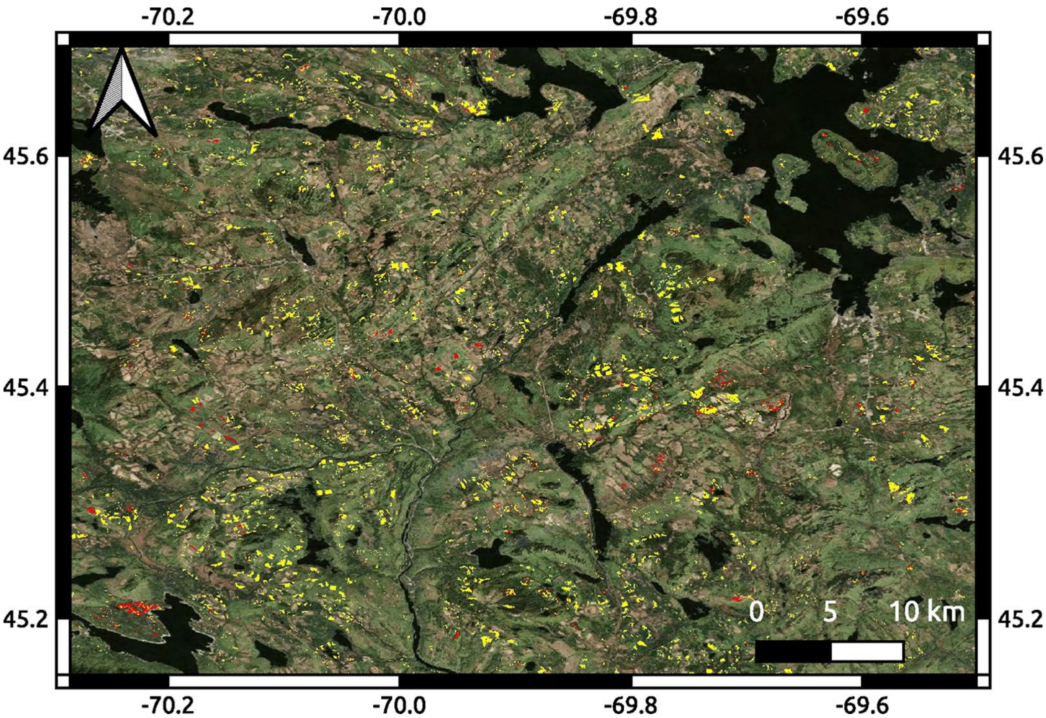

Figure 2: Example of fusing the ALOS-2 backscatter products and GEDI to detect forest disturbances as defined by Forest Change products (Hansen et al., 2013) over a representative region in the new England region. Yellow pixels represent forest disturbance areas detected by backscatter-based estimates, while red pixels indicate disturbed areas as not identified by these estimates.

2.2.2 A modified model considering the natural forest growth

The natural growth of forests remains another concern. In temperate forest regions, the Intact Forest Landscape along with forest height maintain quite stable and only change slightly as trees grow (Potapov et al., 2008; Riofrío et al., 2023). In the New England region, the growth rate was found to be inversely proportional to forest height. This finding i based on a comparison between ICESat-1 or LVIS LiDAR data acquired before 2009 with LVIS LiDAR data collected in 2021. Using these datasets, the temporal evolution of forest height at two epochs is modelled as follows:

$$h_v(t_2) = h_v(t_1) + \alpha \cdot (t_2 - t_1) \quad \textbf{(11)}$$

with the growth rate being expressed as:

$$\alpha = a \cdot h_v(t_1) + b \quad \textbf{(12)}$$

Where a and b are linear coefficients. If a dense time series of forest height data over certain forest land cover is provided, the above equation can be constructed in a differential form as:

https://doi.org/10.5194/essd-2024-596
Preprint. Discussion started: 14 January 2025

$$\frac{\partial h_v}{\partial t} = a \cdot h_v + b \quad \textbf{(13)}$$

This ordinary differential equation yields the following expression:

$$H(t_1) = \left(\frac{b}{a} + H(t_2)\right) e^{-a(t_2 - t_1)} - \frac{b}{a} \quad \textbf{(14)}$$

This expression aligns with the Hossfeld model. However, it requires statistical data on annual growth rates, which is often unavailable on a large scale in practice. When the parameter a is small, Eq. (14) simplifies to the form presented in Eq. (12). Evaluation in the New England region indicates the absolute value of a is less than 0.02. By substituting Equation (12) into the signal model, the following expression is obtained

$$\gamma_{t\&v}^{HV}(t_1) = S(t_1) \cdot \left(\frac{h_v(t2) - b \cdot dt}{(1 - a \cdot dt) \cdot C(t_1)}\right) \quad \textbf{(15)}$$

It follows the model is shifted and scaled with respect to the original model (3).

As a representative example, Figure 3 illustrates the fitted forest growth rate ($\alpha = -0.0134 \cdot h_v(t_1) + 0.464$; unit: $m/year$) for the forest height interval with the highest density at the Harvard Forest site in Massachusetts. This analysis compares LVIS LiDAR data acquired in 2009 and 2021, after filtering out disturbed forests areas ($\alpha \leq -0.1\ m/year$) and short vegetation ($h_v \leq 10\ m$). To illustrate how the InSAR correlation observations from ALOS data are linked to GEDI forest estimates (with time gap of around 10 years), a simulation can be performed by inserting the fitted growth rate into the model (15) and setting $S(t_1) = 0.9$ and $C(t_1) = 11$. Figure 4 presents the simulated results of original sinc model and its modified version. It follows that the forest height below $b \cdot dt$ cannot be well characterized. This value usually ranges from 8 to 15 in the investigation over the New England region. This finding also highlights the importance of utilizing backscatter information to estimate the heights of short forests in this case.

https://doi.org/10.5194/essd-2024-596
Preprint. Discussion started: 14 January 2025

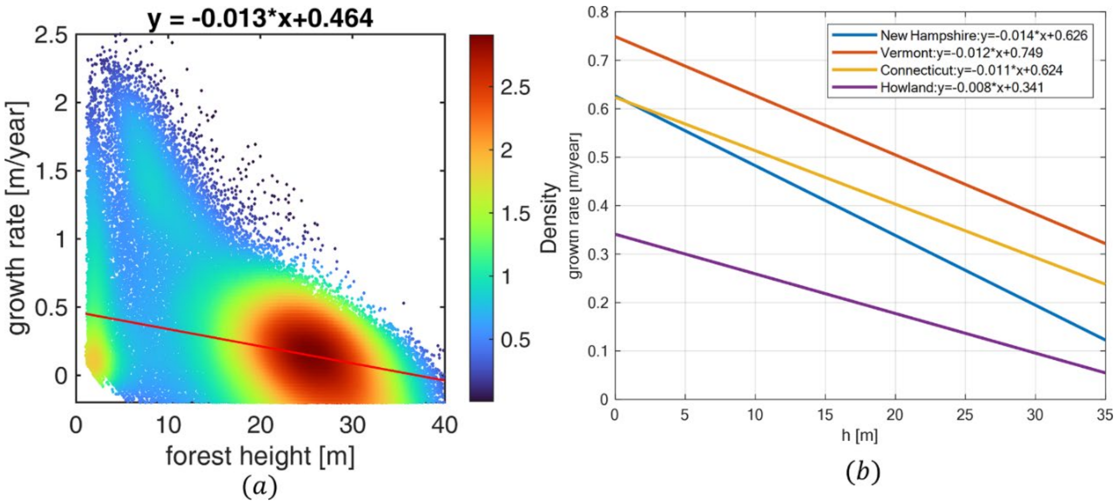

Figure 3: (a) Scatterplot of forest height growth rate versus forest height, derived from a comparison of LVIS forest height estimates between 2009 and 2021 at the Harvard Forest site, Massachusetts. The red line represents the fitted growth rate function of forest height in 2009 over the high-density region. (b) the fitted forest height growth rate functions at typical forest sites of other states in the New England region.

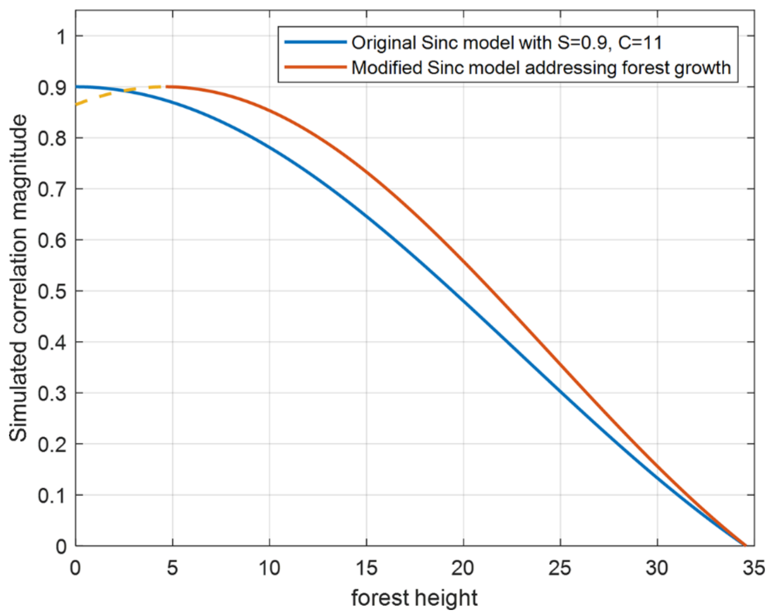

Figure 4: Simulation results comparing the original sinc model and its modified version incorporating natural forest growth at the Harvard Forest site (with forest growth rate function of $\alpha = -0.0134 \cdot h_v(t_1) + 0.464$). The blue line represents the original sinc model with established temporal parameters, while the red line shows the modified model accounting for forest height growth. The dashed orange line highlights the region that cannot be characterized by the modified model.

https://doi.org/10.5194/essd-2024-596
Preprint. Discussion started: 14 January 2025

2.2.3 Approximating the modified model with the original model in the absence of natural growth data

The application of the modified model requires precise statistics of natural growth across various forest types on a large scale. However, this is not available at present, as existing spaceborne LiDAR datasets cannot provide collocated measurements at two different epochs. To maintain consistency with the model under concurrent acquisition condition, the modified sinc model is approximated in the framework of the original sinc model but with updated parameters (S', C'). It is almost impossible to derive S' and C' based on a direct one-to-one analytical transformation between the models (15) and (3). Instead, such parameters can be determined by aligning the original model and modified model at two fixed points. For example, Figure 5 presents the resolved parameters when the alignment is performed for two points at 10 and 30 m for simulating a global fitting case at three typical forest sites, e.g., addressing the whole scene with a large dynamic range of forest heights. The best approximation is observed at the Howland Forest site where the forest height changes slowly. Model mismatches are observed at 20 m at other two Forest sites. This can be addressed by aligning two models for each short interval. Figure 6 presents the behavior of newly fitted parameters when aligning either a short forest interval (e.g., 10–115 m) or a tall forest interval (e.g., 25–30 m). The results suggest that the modified sinc model is better approximated through piecewise fitting, emphasizing the importance of local fitting to accurately represent modified models for a short height range within relatively homogenous forest areas. The S' parameter increase and even exceed 1, particularly for taller trees, suggesting that the original physical definition of $S' \leq 1$ (e.g. only due to moisture-induced dielectric decorrelation in the original model) does not hold any longer. As seen in the behavior of the fitted parameters for each short interval $[x\ x+5]$ in Figure 7, the C' parameters are larger than the original parameter *C* for short vegetation but approach *C* as vegetation height increase. While the S' parameter is close to the original *S* parameter for short trees and become biased for tall trees. For the three forest sites analysed, the White Mountain National Forest shows a larger forest height change rate, leading to a greater deviation between the fitted parameters (S', C') and the original parameters (S, C).

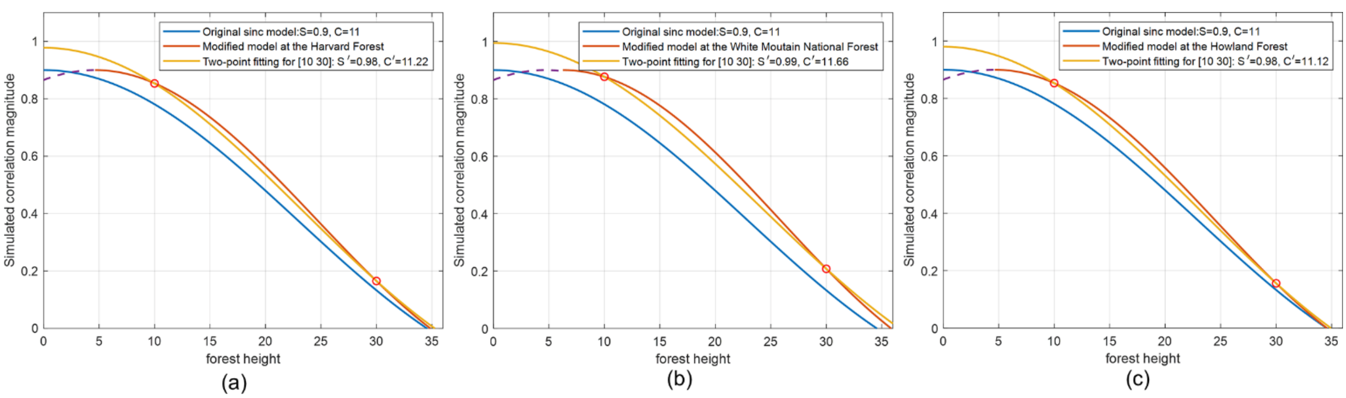

Figure 5: Approximating the modified sinc model with the original model by aligning two points at 10 and 30 m: the newly fitted parameters at (a) Harvard Forest sites; (b) the forest site in Vermont; (c) Howland Forest site.

https://doi.org/10.5194/essd-2024-596
Preprint. Discussion started: 14 January 2025

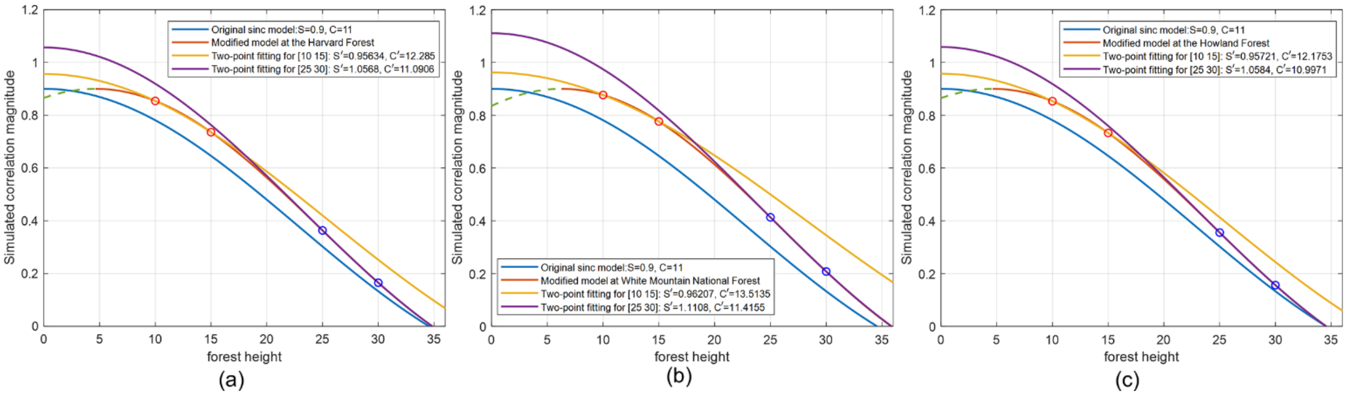

Figure 6: Approximating the modified sinc model with the original model by aligning two points either at 10 and 15 m or at 25 and 30 m: the newly fitted parameters at (a) the Harvard Forest site; (b) the White Mountain National Forest site; (c) the Howland Forest site.

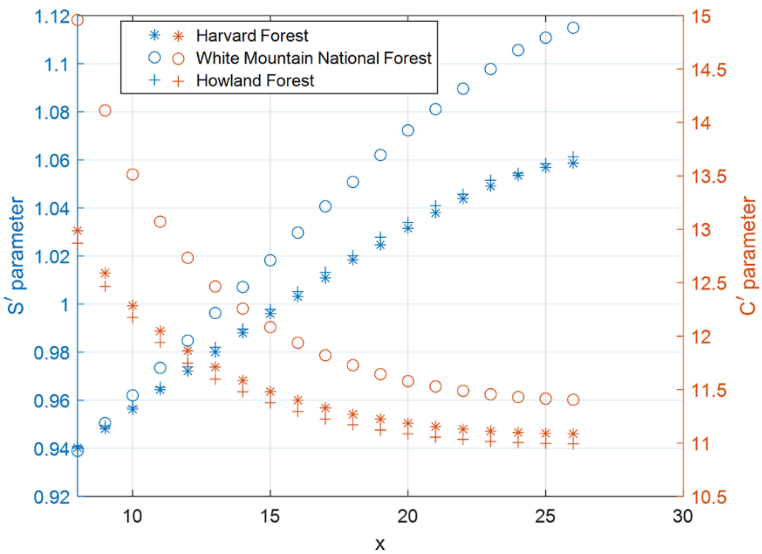

Figure 7: illustration of the dynamic behavior of fitted (S, C) parameters for three representative forest sites when approximating the modified sinc model with original model by local-fitting at fixing points at each forest height interval $[x, x+5]$.

2.3 The selection of proper InSAR pairs

Due to several decorrelation factors (induced by precipitation, human activities, etc.), the temporal decorrelation behavior over forested scenarios is complicated in the context of repeat-pass InSAR. For example, total decorrelation is possible to occur for ALOS-1 InSAR pairs with a temporal span larger than two months during the monsoon season. In this case, the InSAR correlation behavior is dominated by additional decorrelation sources and hence would no longer be well-suited for forest height inversion.

https://doi.org/10.5194/essd-2024-596
Preprint. Discussion started: 14 January 2025

In this context, a pre-inversion metric and a post-inversion error assessment need to be defined when multiple InSAR pairs are available, to eliminate those scenes that would not work well for forest height inversion.

An example of this evaluation is illustrated in Figure 8 and Table 1 below. Here, the fitness of the temporal change model (3) for a given InSAR scene can be evaluated by testing the underlying assumption of the physical scattering model. Specifically, taller trees are more easily decorrelated over time due to the larger deviation of random motions compared to the short ones. A simple yet effective pre-evaluation metric can be attained by linear regression between the GEDI rh98 samples (only keeping forested landcovers) and the coherence magnitude observations. Negative slope in the linear regression usually indicates a relevant validity of the inversion model. As shown in Figure 8 and Table 1, InSAR pairs with a negative slope tend to yield more accurate estimates (e.g., the image pair with slope of -4.86 gives better estimates with respect to the image pairs with of slope higher than -3). Note that while InSAR pairs with short temporal baselines may present higher correlation values, they may not be well-suited to the temporal decorrelation model due to regional precipitation.

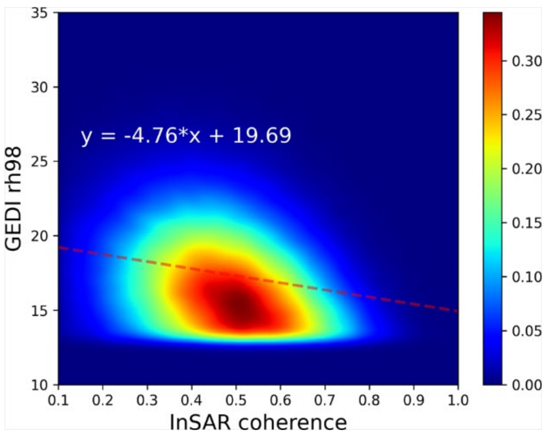

Figure 8: Density scatterplot illustration of relation between repeat-pass ALOS-1 InSAR coherence (3*10 window at 30 m grid) and GEDI rh98, and a red dashed fitted line with the slope as the pre-inversion metric.

https://doi.org/10.5194/essd-2024-596
Preprint. Discussion started: 14 January 2025

Table 1: An example to illustrate the pre-inversion metric (slope) and their inversion performance (Root Mean Square Error (RMSE) and coefficient of determination (R^2) are used here) for the available InSAR pairs in 2007 at the Howland Forest site in Maine, U.S.

InSAR pairs (time vs time)	Slope	RMSE	R^2
20070710-20070825	-2.82	4.09	0.45
20070825-20071010	-2.57	4.14	0.45
20070710-20071010	-4.76	3.8	0.47

The post-inversion metric is defined by using the figure of merit during the local fitting (10): once one pair of temporal parameters ($\{S(i,j), C(i,j)\}$) is determined, a weighted squared summation of the differences between inverted height estimates and GEDI measurements over a regional window is given by

$$\varepsilon(i,j) = \frac{\sum_{(r,c)\epsilon W}\left[w(r,c)\left(\widehat{h_v}(i+r,j+c) - h_{gedi}(i+r,j+c)\right)\right]^2}{\sum_{(r,c)\epsilon W} w(r,c)^2} \tag{16}$$

It can be noted that the derived post-inversion metric $\varepsilon(i,j)$ is also in the same coordinate system as GEDI samples. A Delaunay-triangulation based natural neighborhood interpolation (Park et al., 2006) can be used afterwards to attain pixel-by-pixel evaluation. Such pixel-level evaluation can be used for mosaicking the overlapping areas between consecutive InSAR scenes where overlapping estimates with lower $\varepsilon(i,j)$ are preserved for final map.

It should also be noted that since there are not enough InSAR pairs each year from ALOS-1 due to its 46-day repeat cycle, in this work, we only use the above-mentioned pre- and post-inversion metrics to pick out the best InSAR pair. However, if there are sufficient pairs from more recent spaceborne repeat-pass InSAR missions (such as 12 days for NISAR, 14 days for ALOS-4, and 4-8 days for Lutan-1), a synthetic InSAR coherence map can be generated by applying the monthly, seasonal median, or maximum operation (Kellndorfer et al., 2022).

2.4 Processing workflow

The entire processing workflow is illustrated in Figure 10. provides an example of global-to-local forest height inversion over the Howland Forest site. The standard interferometric preprocessing (including coregistration, topographic phase

https://doi.org/10.5194/essd-2024-596
Preprint. Discussion started: 14 January 2025

compensation, interferometric formation, and geocoding steps) for multiple ALOS-1 InSAR pairs is performed by using JPL's InSAR Scientific Computing Software (ISCE) software (Rosen et al., 2012), in which the parallel computing capabilities of graphic processing units (GPUs) is utilized to enhance the processing efficiency (see (a)). After matching the GEDI samples into the grid of each InSAR scene (the collocated GEDI samples are shown in (b)), the global-to-local inversion for each scene is carried out as follows:

1. **Global Fitting:** As illustrated in subsection 2.1, a global fitting is first performed for obtaining an initial guess of temporal parameters (S_0, C_0) using all the available GEDI rh98 samples and corresponding InSAR observations over each InSAR scene. As noted earlier that a moderate forest disturbance may result in an overestimation of forest height for global fitting (Lei et al., 2017), a re-weighted iterative global fitting is instead used to remove the gross errors induced by forest disturbances after the first iteration.
2. **Local Fitting:** A local fitting is then conducted around each GEDI sample within a local boxcar window with a constraint of smaller searching range in the vicinity of the initial estimates, i.e., $(S \in [S_0 - r_s, S_0 + r_s], C \in [C_0 - r_C, C_0 + r_C])$. Spatial distance based or adaptive weights (e.g., Figure 1) are preferred in local fitting for avoiding much heterogeneous information involved. An expensive computational burden is implied for the local fitting so that a GPU-based implementation (Yu et al., 2019) is developed for enhancing processing efficiency.
3. **Interpolation and Inversion**: the irregularly distributed temporal decorrelation parameters i.e., $\{S(i,j), C(i,j)\}$ are interpolated into the regular grid of InSAR coherence magnitude map based on the Delaunay-triangulation based natural neighborhood interpolation. The forest height is then inverted on a pixel-by-pixel basis using the InSAR coherence observation and the inversion model (resulting in wall-to-wall forest height mapping as shown in Figure 10 (c)).
4. **Backscatter-based Estimates**: The forest height estimates of short vegetation in the previous inversions are replaced by the corresponding backscatter-based estimates (see Figure 10 (d)): the GEDI rh98 samples over bare ground and short vegetation landcovers (e.g., $0 \leq rh98 \leq 10$ m) along with the corresponding backscatter information are fitted using an exponential model, which is then used to obtain backscatter-to-height estimates (Lei et al., 2018). As a rule of thumb, the short trees are identified in this processing via the following criterion i.e., if the backscatter-based forest height inversion is less than 10 m.
5. **Mosaicking**: a selection based mosaicking approach is finally carried out to pick up the best InSAR pairs based on the pre-inversion metric and mosaicking the overlapping area using the pixels with better goodness of fit as discussed in subsection 2.3.

https://doi.org/10.5194/essd-2024-596
Preprint. Discussion started: 14 January 2025

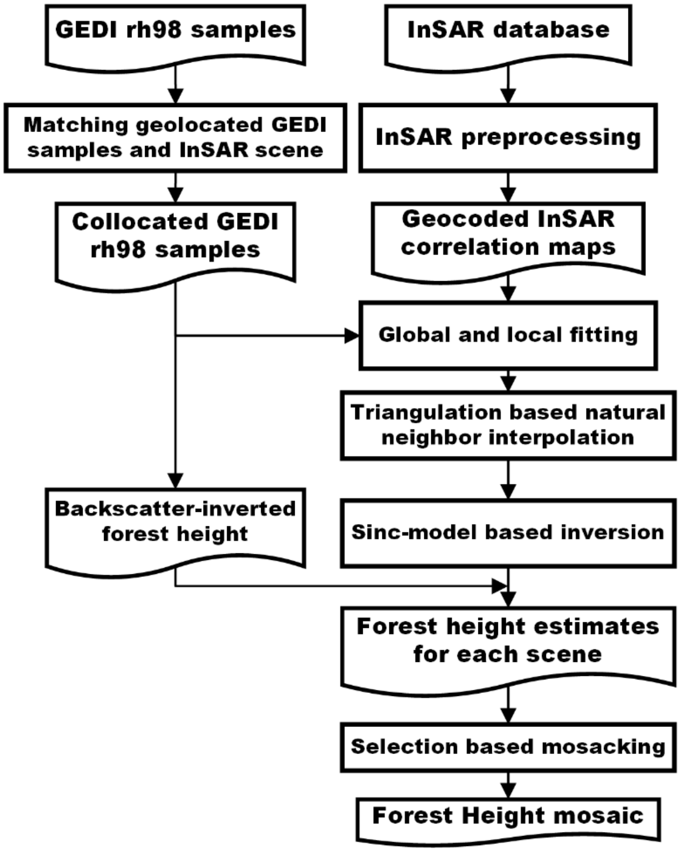

Figure 9: Block diagram of the workflow for generating forest height mosaic.

https://doi.org/10.5194/essd-2024-596
Preprint. Discussion started: 14 January 2025

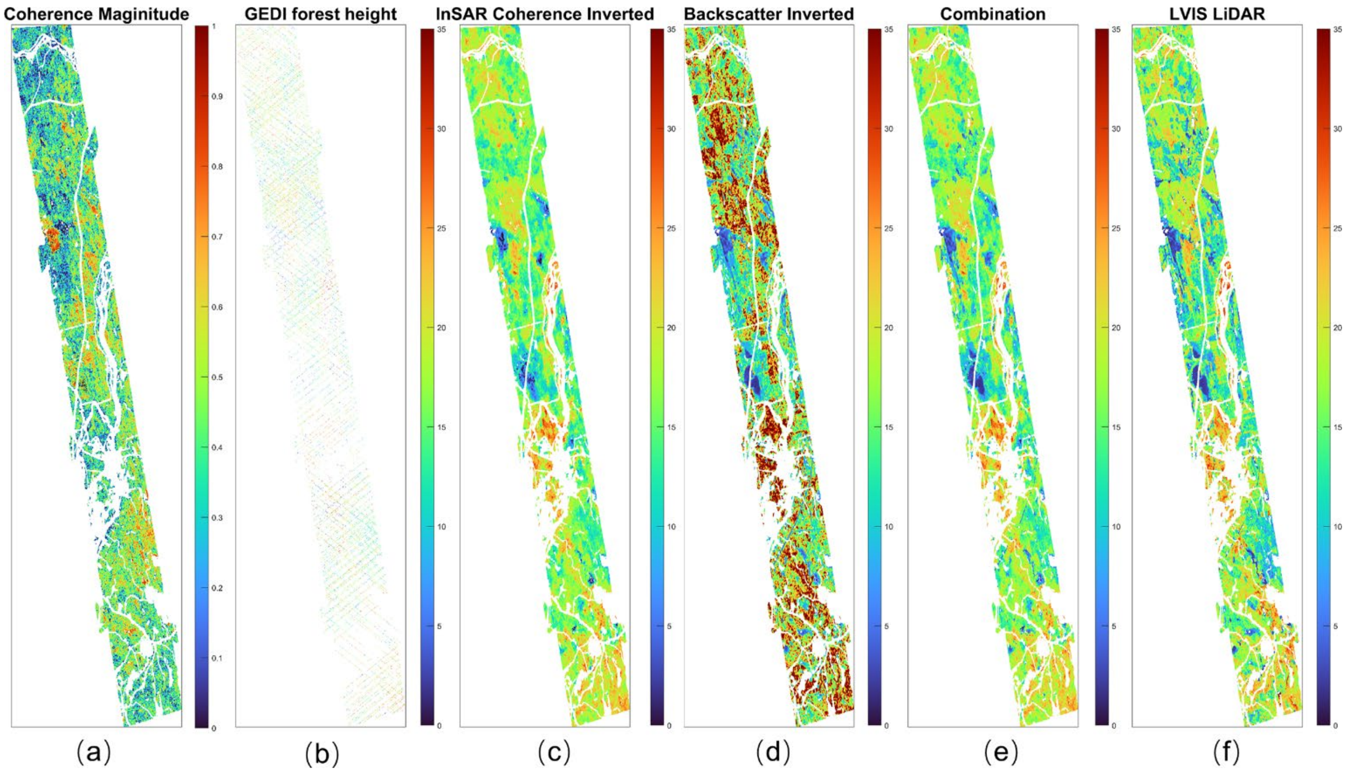

Figure 10 An illustrative example of the processing steps at the Howland Forest site: (a) the input ALOS-1 coherence magnitude map; (b) the GEDI rh98 samples; (c) the forest height estimates based on InSAR coherence information; (d) the backscatter based height estimates; (e) the final forest height map after replacing the estimates of short trees in (c) with the collocated pixels in (d); (f) is the airborne LVIS LiDAR data for validation.

3 Study area and datasets

3.1 Study area

This paper focuses on the northeastern regions of the U.S. and China. These regions contain transitional forests composed of both coniferous and broad-leaved species. As shown in Table 5, the New England region in the northeastern U.S. (including the states of Maine, New Hampshire, Vermont, Massachusetts, Connecticut, and Rhode Island) is selected for the generation and validation of the large-scale mosaic of forest height (covering a total area of 18 million hectares) due to the availability of ample airborne LiDAR datasets. Forests in this area are primarily dominated by coniferous forests (Red Pine, Balsam Fir, Hemlock etc.) and northern hardwoods (Maple, Oak, Beech, etc.). Importantly, the IFL and forest height in these regions maintain stable only with only natural forest growth (Riofrío et al., 2023).

Another large-scale forest height mosaic is also generated over the northeast of China with a total area of 152 million hectares. As shown in Figure 12, the forest height mosaic for China covers five provinces: Hebei, Jilin, Liaoning, Inner

https://doi.org/10.5194/essd-2024-596
Preprint. Discussion started: 14 January 2025

Mongolia and Heilongjiang. Note that Jilin and Inner Mongolia provinces were not fully covered as only forested area within the GEDI observation coverage (<51.6° N) are addressed. The forests in the northeastern China can be primarily classified into four regions: 1) deciduous coniferous forest region located at the northmost parts of Inner Mongolia and Heilongjiang provinces; 2) temperate mixed-forest region (comprising evergreen coniferous and deciduous broad-leaved species) primarily distributed in Heilongjiang and Jilin provinces; 3) northern temperate mixed-forest subregion situated in Liaoning province; and 4) temperate steppe region located partly in Hebei province and partly in Inner Mongolia province.

One reason for selecting the northeastern U.S. and China as the study areas is the availability of extensive airborne LiDAR measurements, including NASA's Land, Vegetation, and Ice Sensor (LVIS) datasets in the U.S. and small-footprint photon-counting LiDAR in China. Another objective for choosing these two regions is to evaluate the performance of forest height inversion in a more comprehensive manner: the New England region of the U.S. was selected for its abundance of GEDI calibration sites, while the northeastern part of China was chosen as a comparable region at a similar latitude but without dedicated GEDI calibration sites.

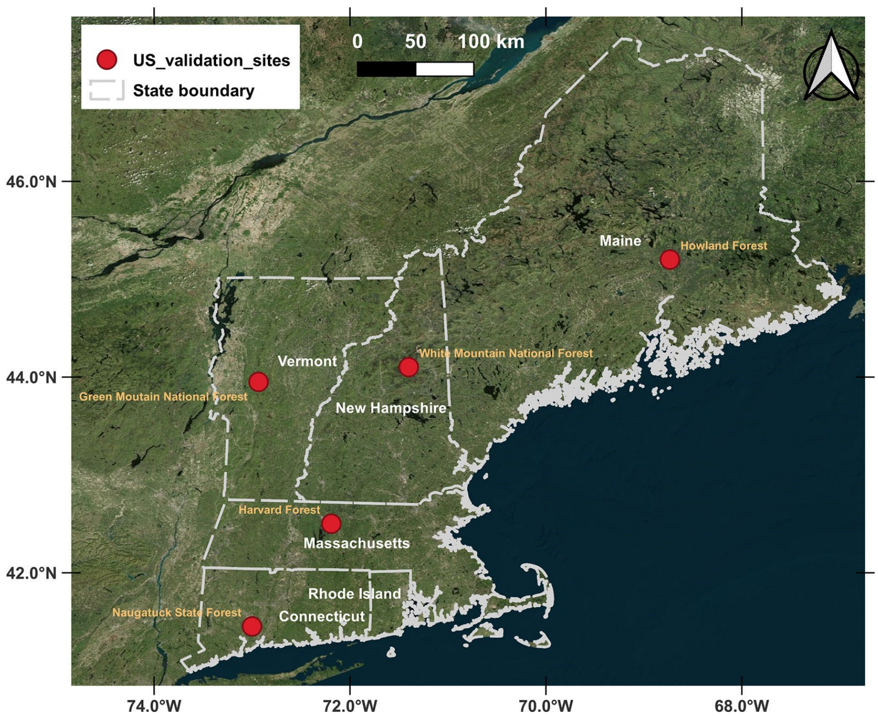

Figure 11: Study area and validation sites for the New England region in the U.S. The generated forest height mosaic map covers the states of Maine, New Hampshire, Massachusetts, Vermont, Connecticut, Rhode Island. The inversion results are validated against the large footprint (25-m) LVIS data acquired either in 2009 or in 2021 over the validation sites (denoted by red dot marker). At White Mountain National Forest site, small footprint GRANIT LiDAR data are also used for validation after reprocessing into equivalent RH98 metric map. The features of the validation sites are summarized in Table 2.

https://doi.org/10.5194/essd-2024-596
Preprint. Discussion started: 14 January 2025

Several experimental and validation sites are selected across the northeastern regions of the U.S. and China, with their relevant information summarized in Table 2 and Table 3, respectively. In the New England region, validation is conducted at various sites including the Howland Forest site in Maine, Harvard Forest site in Massachusetts, the White Mountain National Forest (WMNF) site in New Hampshire, the Green Mountain National Forest (GMNF) site in Vermont, and the Naugatuck state forest site in Connecticut. These forest validation sites are covered by medium footprint (25 m) LVIS data acquired either in 2009 or in 2021. Additionally, the forest height inversion over the WMNF site was evaluated using GRANIT airborne laser scanning (ALS) data acquired in 2011 (Haans et al., 2009), with the canopy height product extracted from the waveform data at a raster sampling spacing of 2 m.

Regarding the northeastern region of China, evaluation was performed at one forest site in each province: the Mengjiagang Forest site in Heilongjiang province, the Dagujia Forest site in Jilin province, the Saihanba Forest site in Hebei province, the Hubao national park in Jilin province, and the Genhe Forest Bureau in Inner Mongolia province. Validation of the forest height product across all the forest validation sites in China was done by comparing against the small footprint (0.5 to 1 m) ALS data.

To provide a preliminary assessment of forest change in these two regions, forest loss maps derived from global forest change products (Hansen et al., 2013) are shown in Figures 13 and 14.

https://doi.org/10.5194/essd-2024-596
Preprint. Discussion started: 14 January 2025

Figure 12: Study area and validation sites in the northeastern China. Five provinces are covered in the generated forest height mosaic: Jilin, Liaoning, Hebei, Heilongjiang, Inner Mongolia. The performance of the forest height inversion is assessed by comparing against small footprint (0.5-m to 1-m) LiDAR data at the validation forest sites (as indicated by the red diamond markers) in each province. The features of the validation sites are summarized in Table 3.

Table 2 Forest validation sites covered by the airborne LiDAR observation in the New England, U.S

Validation sites	Location	Dominated tree species	LiDAR data acquisition year	Slope statistics
Howland Forest	68°44′ W, 45°12′N	Red spruce (Picea rubens Sarg.) and eastern hemlock	2009	Mean: 2.3° STD: 5.3
Harvard Forest	72°11′W, 42°31′N	Red oak, Red maple, Black birch, White pine, Eastern hemlocc	2021	Mean: 5.5° STD: 4.6°
White Mountain National Forest	71°18′W, 44°6′N	Red Spruce, Eastern Hemlock, American Beech, and Red Maple,	2011	Mean: 9.7° STD: 8.6°
Green Mountain National Forest	73°04′W	Sugar maple, American beech, red maple, yellow and paper birch	2021	Mean: 10.4° STD: 7.6°
Naugatuck State Forest	73°00′W 41°27′N	Northern red oak, Mixed upland hardwoods, Yellow-poplar	2021	Mean: 5.2° STD: 4.5°

https://doi.org/10.5194/essd-2024-596
Preprint. Discussion started: 14 January 2025

Table 3 The forest validation sites covered by the ALS validation data in the northeastern China

Validation sites	Location	Dominated tree species	LiDAR data acquisition year	Slope statistics
Mengjiagang forest	130°42′ E, 46° 25′ N	Coniferous plantations (Larix gmelinii and Pinus syvestris)	2017	Mean: 6.6° STD: 5.6°
Dagujia forest	125° 00′ E, 43° 21′ N	Coniferous plantations (Larix kaempferi, Pinus koraiensis, etc)	2018	Mean: 13.5° STD: 7.4°
Saihanba forest	117° 18′ E, 42° 24′ N	Larix principis-rupprechtii, Pinus syvestris, and Betula	2018	Mean: 8.7° STD: 7.3°
Genhe forest bureau	121° 32′ E, 50° 47′ N	Larix gmelinii, Betula platyphylla, Populus davidiana	2022	Mean: 7.0° STD: 5.4°
Hubao national park	130° 12′ E, 43° 28′ N	Mongolian oak, Basswood, Betula platyphylla	2018	Mean: 8.7° STD: 7.4°

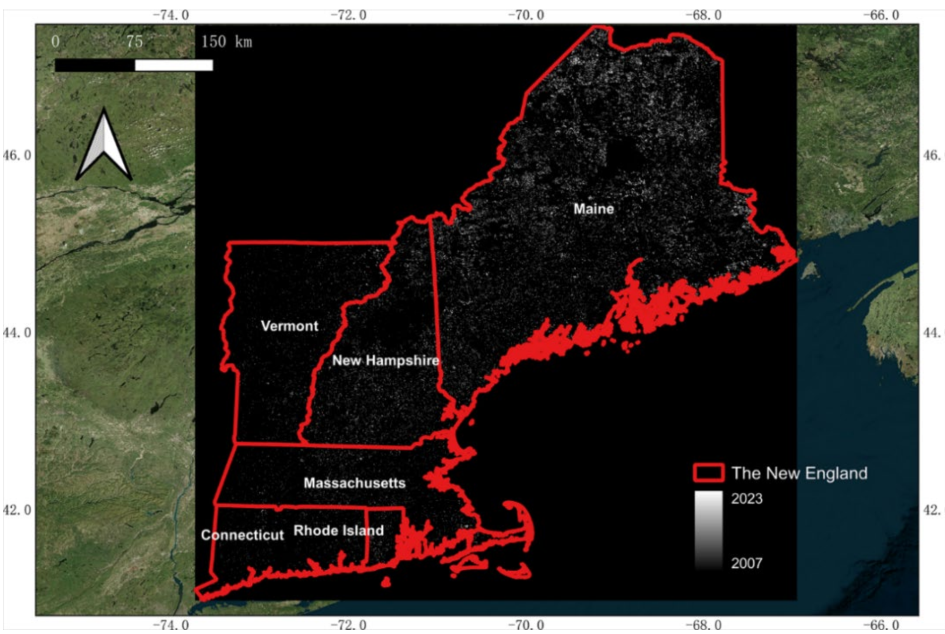

Figure **13 The map of forest loss occurred from 2007 to 2023 within the New England region based on the global forest change product (Hansen et al., 2013).**

https://doi.org/10.5194/essd-2024-596
Preprint. Discussion started: 14 January 2025

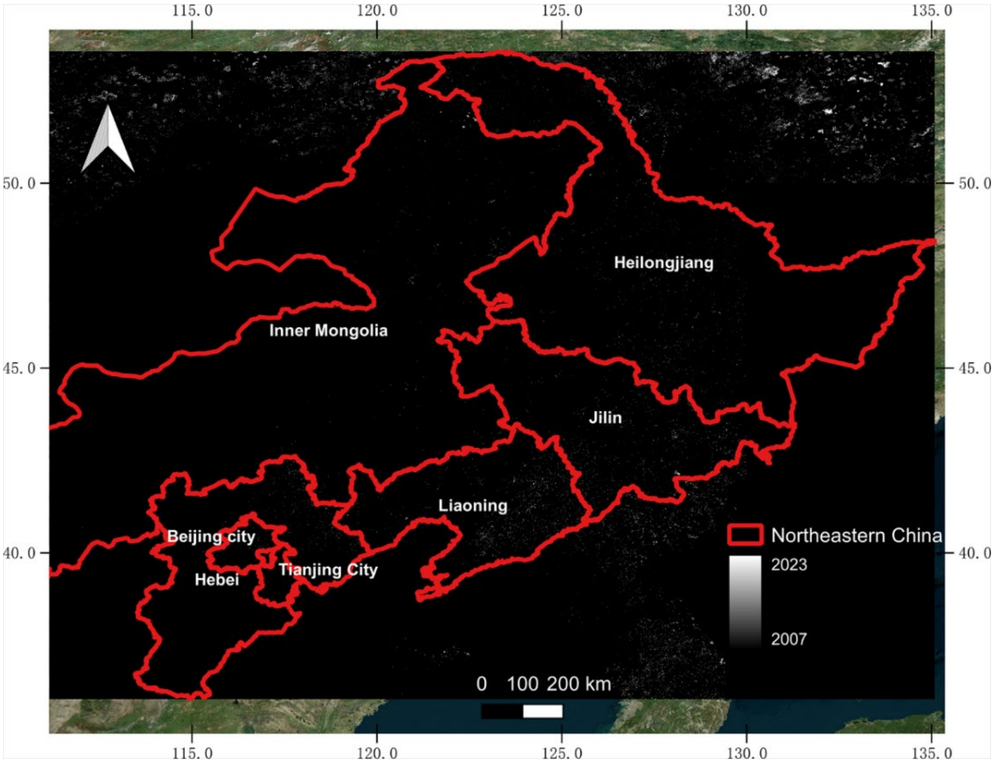

Figure 14 The forest loss occurred from 2007 to 2023 within the northeastern China based on the global forest change products(Hansen et al., 2013)

3.2 Spaceborne and Airborne Remote Sensing datasets

3.2.1 Spaceborne InSAR Datasets

The freely accessible L-band InSAR data from Japanese Aerospace Exploration Agency (JAXA)'s Advanced Land Observing Satellite (ALOS) mission were used for generating the InSAR correlation observations. In addition, a few radar data from ALOS-2 (a follow-up mission of ALOS-1) were also employed as case studies for validating the fusion of radar-lidar under concurrent condition. Furthermore, the spaceborne LiDAR waveform-based metrics (rh98 as a proxy of forest height) from GEDI mission were used for parameterizing the temporal decorrelation model.

Global Fine Beam Dual-polarization (FBD) SAR images with spatial grid of (10 × 3 m for range and azimuth directions) were collected by ALOS satellite from 2007 to 2010, with a repeat cycle of 46 days. To generate forest height mosaic, 100 cross-polarized ALOS-1 InSAR scenes (identified by one pair of frame and orbit numbers) were processed to cover the New England region in the U.S., whereas more than 600 InSAR scenes were processed for covering the northeast of China. The InSAR preprocessing was done by JPL's ISCE software. It was reported by (Lei and Siqueira, 2014) that the ALOS-1 InSAR observations acquired during the summer/fall time frame of 2007 and 2010 tended to have higher InSAR coherence.

https://doi.org/10.5194/essd-2024-596
Preprint. Discussion started: 14 January 2025

In the practical processing, multiple cross-polarized interferograms during the lifetime of ALOS-1 (2007-2011) were formed and processed for each scene based on different combinations of acquisition dates, allowing for the identification of the best InSAR pair for each ALOS-1 observation scene.

As a follow-on mission to ALOS-1, ALOS-2 had a shorter revisiting period (14 days), resulting in a better InSAR correlation behavior. The acquisition started from 2016, allowing for a nearly concurrent observations with respect to GEDI samples. However, the acquisition strategy and limited access to the high-resolution dual-polarized strip-map data have made it more difficult to form proper InSAR pairs and perform large-scale mapping. The grid of ALOS-2 image in FBD mode is at a grid of 8 × 4 m for range and azimuth directions. A windows size of 4 × 8 looks is used for the coherence estimation, resulting in an averaged pixel size of 30 m.

In this study, the use of limited ALOS-2 data is devoted for demonstrating the proposed approach under ideal case. The large-scale mapping capabilities were demonstrated using free-access ALOS data over the temperate forest regions. It is also noted that there is time discrepancy between the acquisition dates of ALOS and GEDI. This discrepancy is addressed using the two-fold solution as detailed in Section 2.2. As for the abrupt discrepancy due to forest disturbance (e.g. logging, deforestation, and fire) that usually results in no/short vegetation with small backscatter values, replacing the InSAR inverted forest estimates with those derived from the appropriate ALOS-2 backscatter mosaic map for short vegetation (as shown in subsection 2.2.1) can detect the disturbed forest areas. And the study area is mainly concentrated on temperate and boreal forests, the heights of mature temperate forests (intact forest landscape) remain almost stable with slight change. Nevertheless, a simulation in subsection 2.2.3 shows the approach of this study can approximate the height of the forests subject to natural growth at regional scale. In other words, all the InSAR based height inversions are calibrated to the acquisition time of GEDI, and thus best compared with the concurrent airborne LiDAR validation data.

3.2.2 Spaceborne LiDAR Datasets

As the first spaceborne LiDAR mission to characterize ecosystem structure and its dynamic, the NASA's GEDI mission was launched in December 2018. GEDI provides near-global measurements of forest structure metrics from 51.6° S to 51.6° N until 2024. With three lasers mounted, eight parallel tracks of samples at a footprint of 25 m are simultaneously collected. The spatial separation between samples during one datatake is 60 m in the along-track direction and 600 m in cross-track direction. The GEDI rh98 metric is selected as an appropriate proxy for indicating forest canopy height within each footprint because it has less sensitivity to errors as compared to the rh100 metric (Hofton et al., 2020). After filtering out GEDI samples with less penetration sensitivities (e.g., 95% sensitivity, 50 m maximum elevation difference between GEDI and TanDEM-X measurements), the remaining L2A version 2 GEDI samples are used for calibrating the inversion model.

https://doi.org/10.5194/essd-2024-596
Preprint. Discussion started: 14 January 2025

3.2.3 Airborne LiDAR data

3.2.3.1 Medium-footprint LiDAR data

A significant amount of airborne full-waveform LiDAR data was collected across the U.S. using LVIS sensor. The LiDAR data were processed into rh98 maps at 25 m grid. Specifically, LiDAR data over the Howland Forest site in Maine were obtained in 2009. LVIS data acquired in 2021 for GEDI calibration cover all the other forest sites in the New England region, which were classified into four parts based on the state boundaries of New Hampshire, Vermont, Massachusetts, and Connecticut.

3.2.3.2 Small footprint LiDAR data

In some cases, small footprint LiDAR data have to be used for validating the inversion. The validation at the WNMF site utilized GRANIT LiDAR data, which has a 2 m footprint and was acquired in 2011. All the forest heights in the northeastern China were validated using small footprint LiDAR data. The airborne LiDAR data, with an average point density of 6 pts/m² over Hubao National Park, were acquired using an airborne LiDAR system owned by the Chinese Academy of Forest Inventory and Planning. The observations covering all other forest sites in the northeastern China were acquired during 2017-2022 using the airborne remote sensing system developed by the Chinese Academy of Forestry (Pang et al., 2016), which has an average point density of 12 pts/m². It should be noted that validating the forest height estimates against airborne LVIS observations is not straightforward, as the footprint of these airborne data is much smaller than the footprint of GEDI. . To address this footprint difference, an equivalent RH98 metric (referred to as ERH98 hereafter) needs to be extracted at the position of the 98th percentile of the LiDAR waveform or from the histogram formed by high-resolution CHM estimates within a 25 m footprint. Following this procedure, all small-footprint LiDAR data were reprocessed to generate forest height estimates based on the ERH98 metric with the same footprint size.

3.2.4 Forest and Non-forest Maps

Non-forest areas including water bodies and urban areas were masked out using the 2021 National Land Cover Database (Homer et al., 2015) and the 2021 ESRI Global Land Cover Map (Karra et al., 2021).

3.2.5 Backscatter mosaic map

This study used the global radar backscatter products generated by JAXA using ALOS-1/2 FBD images (Shimada et al., 2016) after radiometric and geometric calibration (including slope effects correction). Specifically, the global cross-polarized backscatter products from 2019 and 2020 over the northeast of the U.S. and China were utilized to obtain height estimates of short vegetation. The two-year products were used to account for missing data gaps, backscatter calibration inconsistencies, and to best match the acquisition time of the validation airborne LiDAR data.

4 Results

This section begins by presenting large-scale forest height mosaic maps for the northeastern regions of the U.S. and China, and is followed by extensive validation for representative individual forest sites within these regions.

4.1 Forest Height mosaic generation

The proposed inversion approach was developed as an automated open-source software, serving as version 2 of the Forest Stand Height (FSH) software (https://github.com/Yanghai717/FSHv2).

For generating the forest height mosaic map over the New England region (a total area of 18 million hectares), over 100 ALOS-1 InSAR scenes were processed using a multi-look averaging (two range looks and ten azimuth looks leading to a pixel size of 20 by 30 m consistent with SRTM grid) and ~15 million GEDI rh98 samples were used for model parametrization. The height estimates of short vegetation were replaced with the backscatter-based estimates using the ALOS-2 backscatter products in either 2019 or 2021. A few ALOS-2 InSAR pairs were also used for demonstrating the fusion of radar-lidar under concurrent acqusition. Non-forest areas were masked out based on the 2021 NLCD products. The mosaic was projected to the same geographic coordinate grid of SRTM DEM product. The forest height mosaic is depicted in Figure 15. The absence of discontinuity between adjacent scenes confirms the consistency of the forest height estimates. Additionally, the coastal region is included in the inversion, despite potential challenges posed by weather conditions (as reported in Lei et al., 2018). This underscores the advantage of using the global-to-local two-stage inversion approach to handle fast spatially-varying temporal change factors induced by different land covers or weather/climate conditions. Further quantitative evaluation is conducted in subsequent sections, with a focus on each individual forest site.

For the northeast of China, 688 ALOS-1 InSAR scenes and 160 million GEDI samples were used to generate the mosaic covering the five provinces (total area of 152 million hectares). Non-forested areas were masked out based on the 2021 ERSI global land cover maps. ALOS2 global backscatter maps for 2019 and 2020 were employed to estimate the height of short trees to match the acquisition time of the validation airborne LiDAR data. The final forest height mosaic is shown in Figure 16. It is noted the area outside the coverage of GEDI observation (>51.6°N) were discarded. The generated products are made available via https://doi.org/10.5281/zenodo.11640299 (Yu and Lei, 2024). Further evaluation is shown in subsection 4.2.

https://doi.org/10.5194/essd-2024-596
Preprint. Discussion started: 14 January 2025

Open Access Earth System Science Data Discussions

560 In both cases, small values of κ_z are maintained for all available InSAR pairs (κ_z are below 0.15 rad/m, and the mean values are 0.032 rad/m and 0.029 rad/m for Chinese and American datasets, respectively) which is conformed to the assumption made in (Lei and Siqueira, 2014).

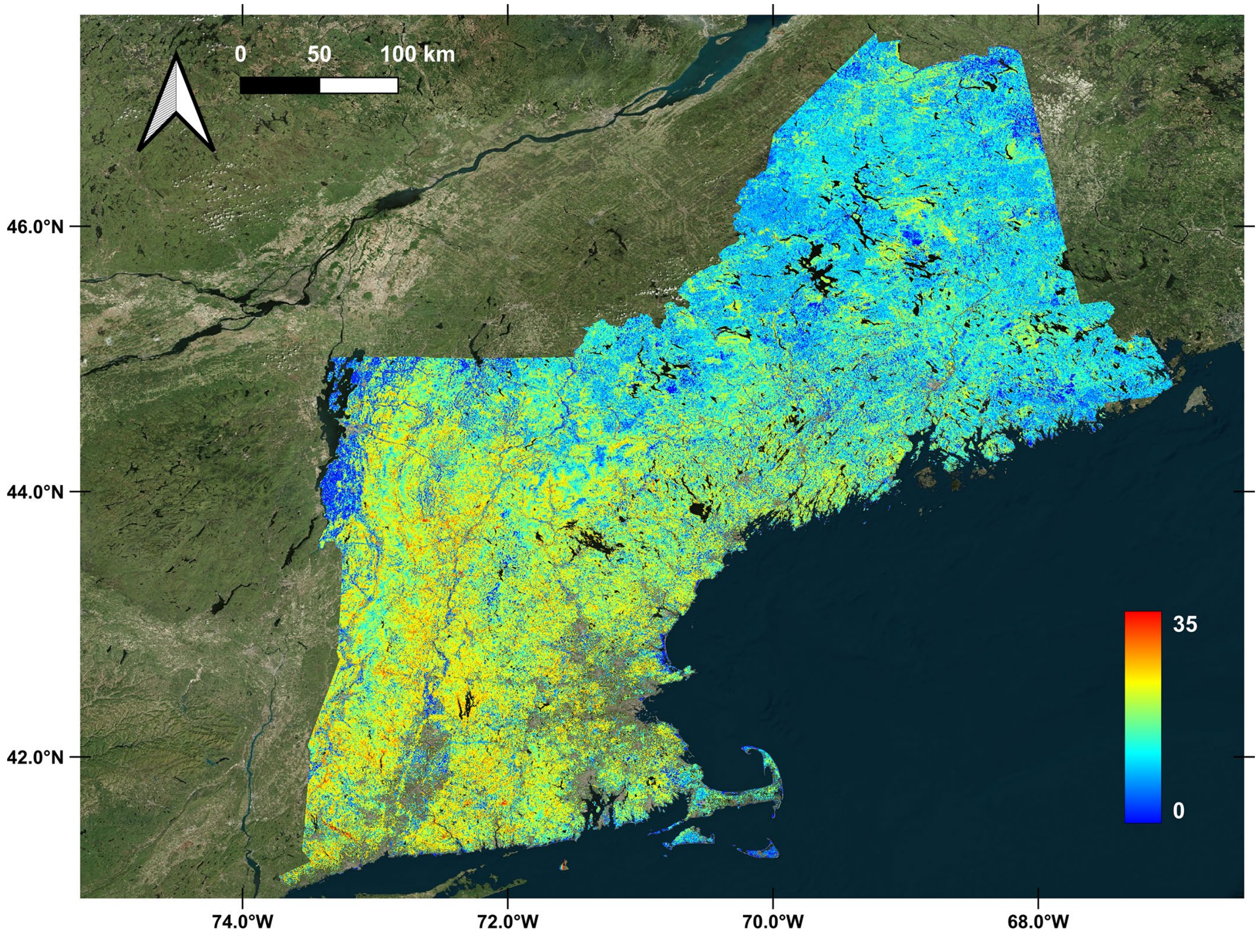

565 **Figure 15 30 m gridded forest height mosaic map based on ALOS-1 InSAR and GEDI RH98 metric for the New England region in the U.S., with a total area of 18million hectares. The color map ranges from 0 m ("blue" for bare surfaces) to 35 m ("red" for tall trees). It was projected onto the map coordinate of SRTM DEM products.**

https://doi.org/10.5194/essd-2024-596
Preprint. Discussion started: 14 January 2025

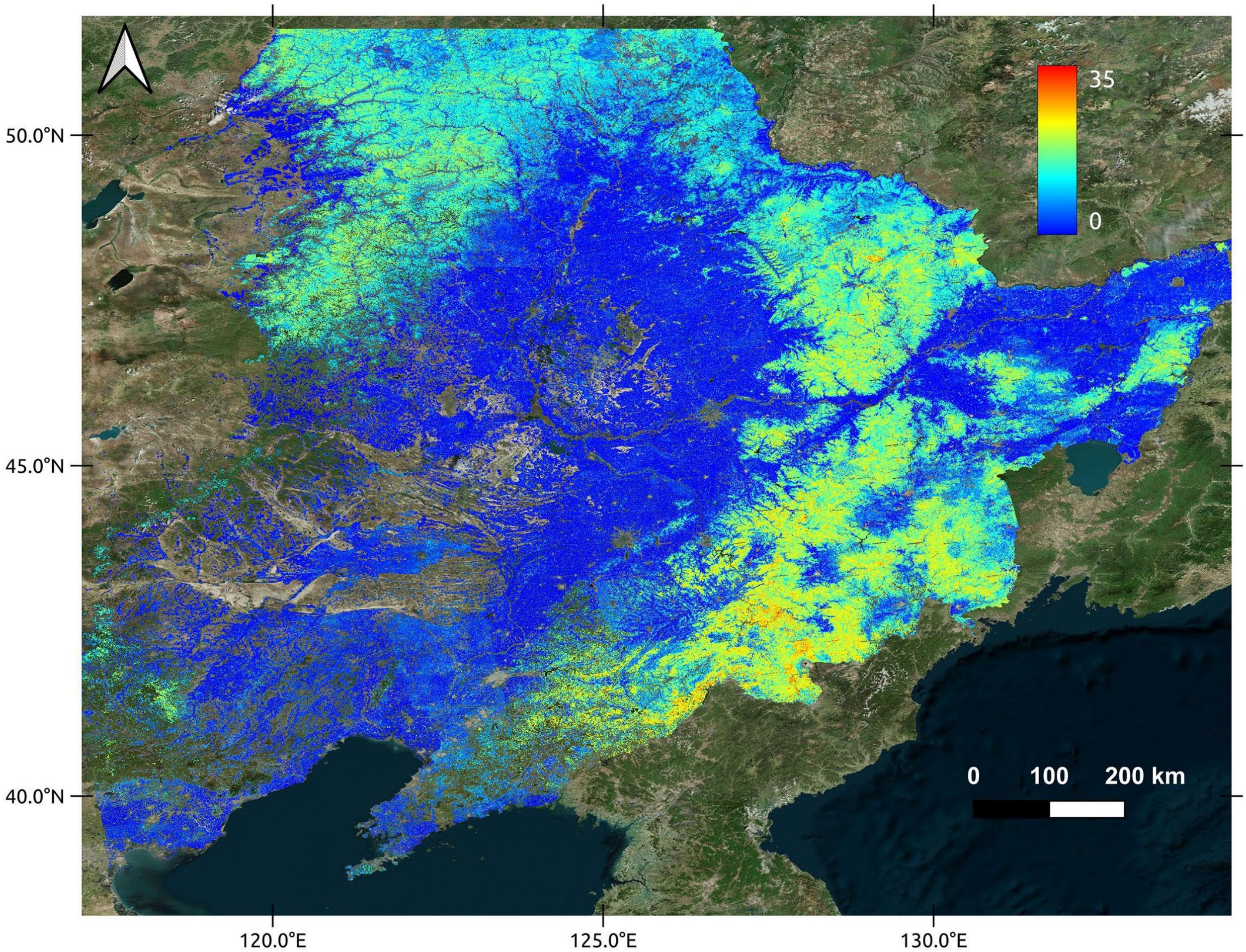

Figure 16: 30 m gridded Forest height mosaic map based on ALOS-1 InSAR and GEDI RH98 metric for the northeastern region of China, with a total area of 152 million hectares.

4.2 Validation over the New England region

This subsection focuses on validation of the forest height inversion at each representative test site in the New England, U.S. Two case studies over the Howland and Harvard Forest sites are presented initially to assess the inversion over relatively flat surfaces. The evaluation is then extended to the WMNF site, where small footprint LiDAR are used for validation.

4.2.1 Howland Forest site

The Howland Forest was selected as one of the test sites, continuing from previous efforts in developing the inversion approaches (Lei et al., 2018; Lei and Siqueira, 2022). Comparing results from these earlier studies with the current one

https://doi.org/10.5194/essd-2024-596
Preprint. Discussion started: 14 January 2025

allows for an evaluation of performance improvements. A strip of LVIS LiDAR data acquired in 2009 was used as the reference to assess the inversion accuracy of both the ALOS-1-based forest height mosaic map and the ALOS-2-based inversion from a single pair of ALOS-2 data (frame: 890, orbit: 37).

The comparison between the inverted forest height estimates and the LVIS LiDAR data is illustrated in Figure 17: Validation of forest height inversion at the Howland Forest: (a) LVIS RH98 (25 m footprint acquired in 2009), (b) inversion extracted from ALOS-1 mosaic (c) ALOS-2 based inversion, and the difference maps of (d) ALOS-1 based inversion versus LVIS data and (e) ALOS-2 based inversion versus LVIS data., featuring the differential height maps between the inversion and the LiDAR data (Figure 17 (d) and (e)). After aggregating the pixels of the inversion and validation maps into 0.8 hectare units (3 by 3 pixels) by averaging, scatterplots of the comparisons are provided in Figure 18 for a quantitative interpretation. Four error metrics were used for statistical evaluation of the inversions: the coefficient of determination (R^2), Root Mean Square Error (RMSE), Bias, and Standard Deviation. Unless otherwise specified, all the scatterplots of comparisons and the derived error metrics presented in this paper are based on an aggregated pixel size of 0.8 hectare.

The comparison indicates that the ALOS-1-based mosaic inversion can estimate forest height with an RMSE of 3.8 m. Due to the better correlation behavior achieved with a 14-day temporal baseline, the ALOS-2-based single scene inversion achieves a forest height accuracy with an RMSE of 3.6 m. In previous efforts, the accuracy of forest height inversion was reported as an RMSE of 4 m at a 6.25-hectare aggregated pixel size. Thanks to the availability of extensive GEDI samples and the global-to-local two-stage inversion approach, the algorithm achieves a significantly improved inversion accuracy, even at a finer grid.

Indeed, the dense spatial distribution of GEDI samples allows for finer characterization of temporal factors (S, C), as shown in Figure 19. As predicted in subsection 2.2.3, the saturation behavior of S parameters is due to the approximating of the modified model with natural forest growth (15) using the original model (3) in the local window with taller forests. This approach, which fuses SAR information with GEDI samples, not only addresses the wall-to-wall mapping issue inherent in the discrete sampling of GEDI observations but also enhances the accuracy of forest height inversion. As shown in Figure 20, the 30 m interpolated GEDI based forest height maps still face discontinuity problems. However, by incorporating ALOS-2 InSAR coherence observations, an accuracy improvement of up to 20% has been achieved.

https://doi.org/10.5194/essd-2024-596
Preprint. Discussion started: 14 January 2025

Open Access Earth System Science Data Discussions

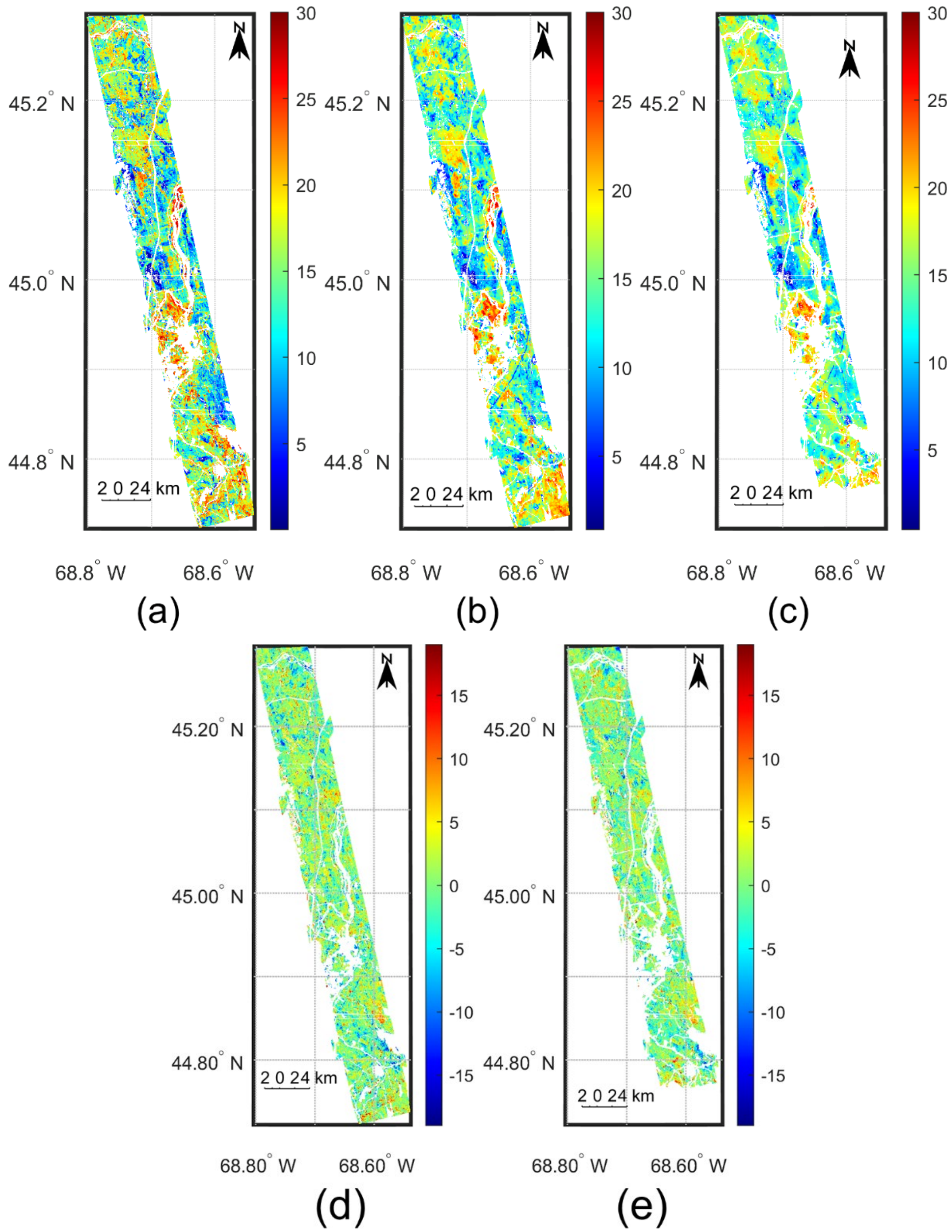

610 **Figure 17: Validation of forest height inversion at the Howland Forest: (a) LVIS RH98 (25 m footprint acquired in 2009), (b) inversion extracted from ALOS-1 mosaic (c) ALOS-2 based inversion, and the difference maps of (d) ALOS-1 based inversion versus LVIS data and (e) ALOS-2 based inversion versus LVIS data.**

https://doi.org/10.5194/essd-2024-596
Preprint. Discussion started: 14 January 2025

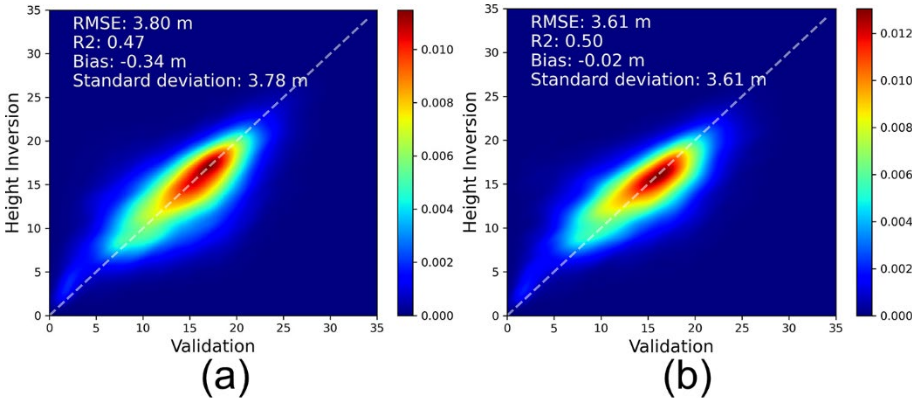

615 **Figure 18: Density scatterplots of forest height inversion at the Howland Forest site for (a) ALOS-1 mosaic versus LVIS LiDAR, and (b) ALOS-2 single scene versus LVIS LiDAR.**

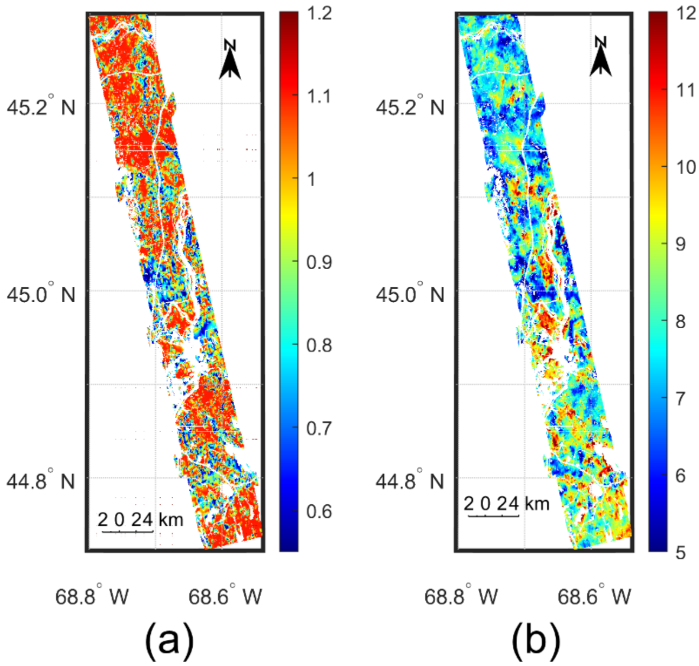

Figure 19: the interpolated maps of temporal change parameters for (a) *S* and (b) *C*

620

https://doi.org/10.5194/essd-2024-596
Preprint. Discussion started: 14 January 2025

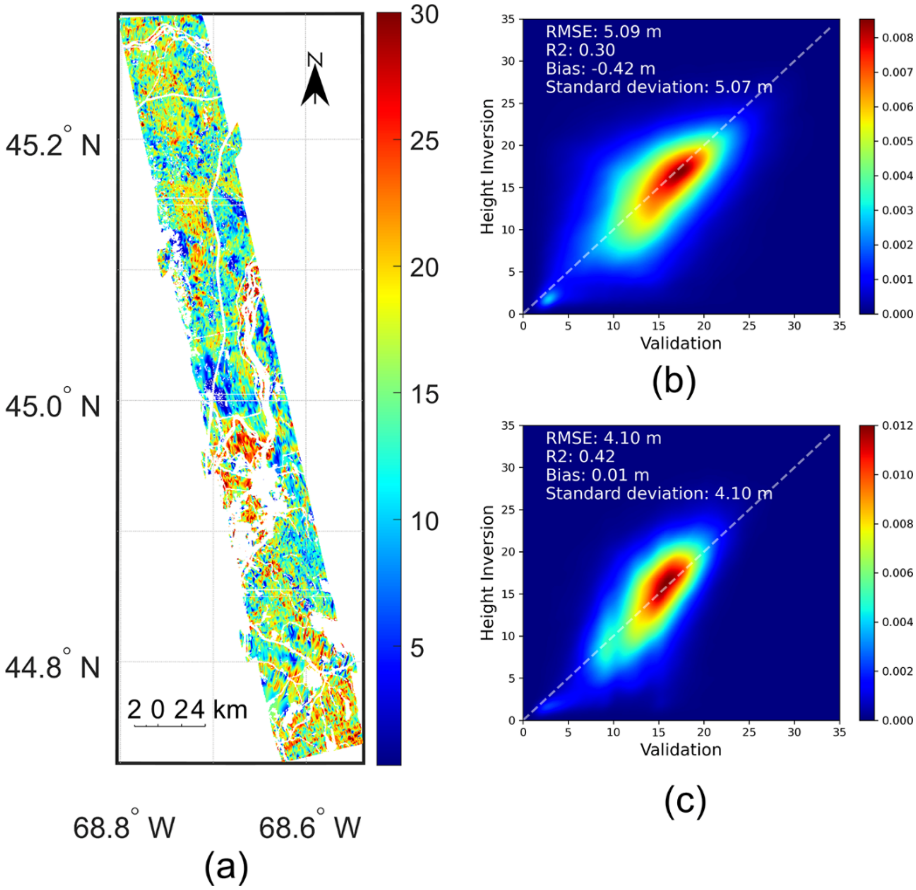

Figure 20: (a) 30 m gridded interpolated GEDI height map and (b) density scatterplots comparing 30 m interpolated GEDI map and LVIS LiDAR data (c) density scatterplots comparing ALOS-2 based inversion with LVIS LiDAR data. Both (b) and (c) were created at the raw pixel size of 30 m.

4.2.2 Harvard Forest site

The Harvard Forest was selected to evaluate the inversion in a region characterized by high biomass, up to 400 Mg/ha (Tang et al., 2021). Figure 21 presents the LVIS validation data acquired in 2021, covering the Harvard Forest area in subfigure (a), and the forest height estimates extracted from the ALOS-1 mosaic and the ALOS-2 single-scene inversion results (frame: 2770, orbit: 141) in subfigures (b) and (c). The comparison of ALOS-1 and ALOS-2 inversion results against the validation data is illustrated in the differential height maps in Figure 22. The density scatterplots from these two comparisons are given in Figure 23.

https://doi.org/10.5194/essd-2024-596
Preprint. Discussion started: 14 January 2025

Both the ALOS-1 mosaic and ALOS-2 single-scene inversion are capable of estimating forest height with an RMSE of 4 m. The biased estimation occurred in taller forest stands may be attributed to the degraded sensitivities of GEDI measurements for dense tall forest stands (Fayad et al., 2022).

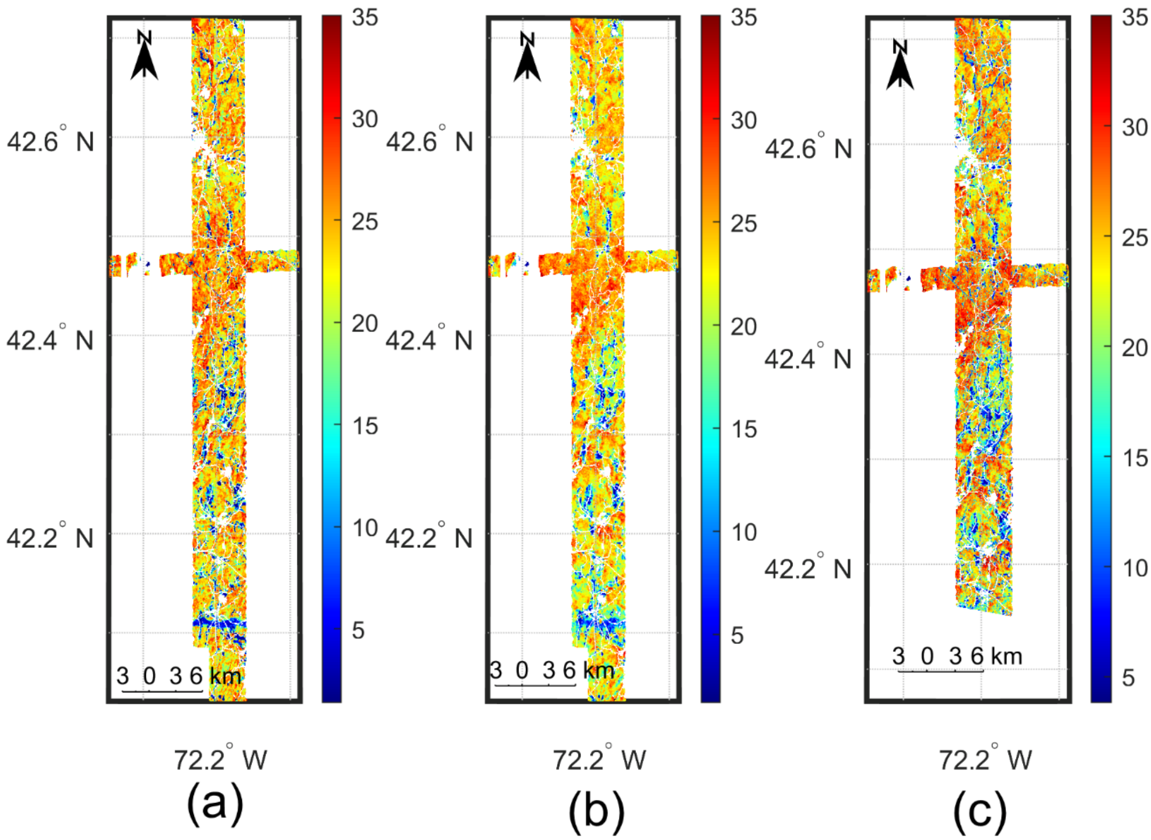

Figure 21: Validation of 30 m gridded forest height inversion at the Harvard Forest site: (a) LVIS LiDAR RH98, (b) ALOS-1 based estimates (c) ALOS-2 based inversion.

https://doi.org/10.5194/essd-2024-596
Preprint. Discussion started: 14 January 2025

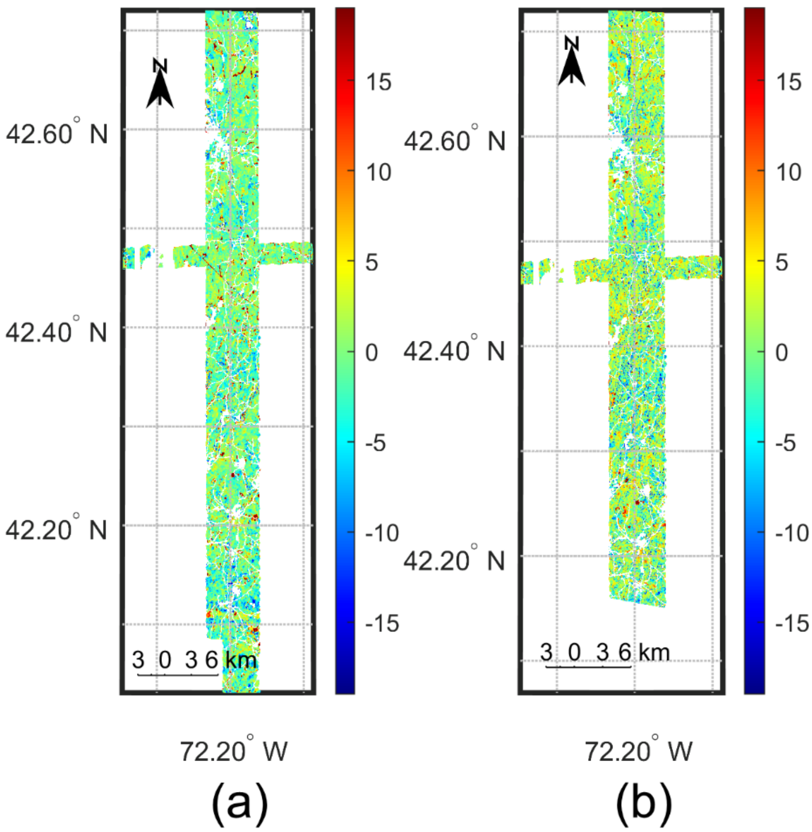

Figure 22: Differential height maps over the Harvard Forest site: (a) ALOS-1 mosaic versus LVIS LiDAR, and (b) ALOS-2 single scene versus LVIS LiDAR.

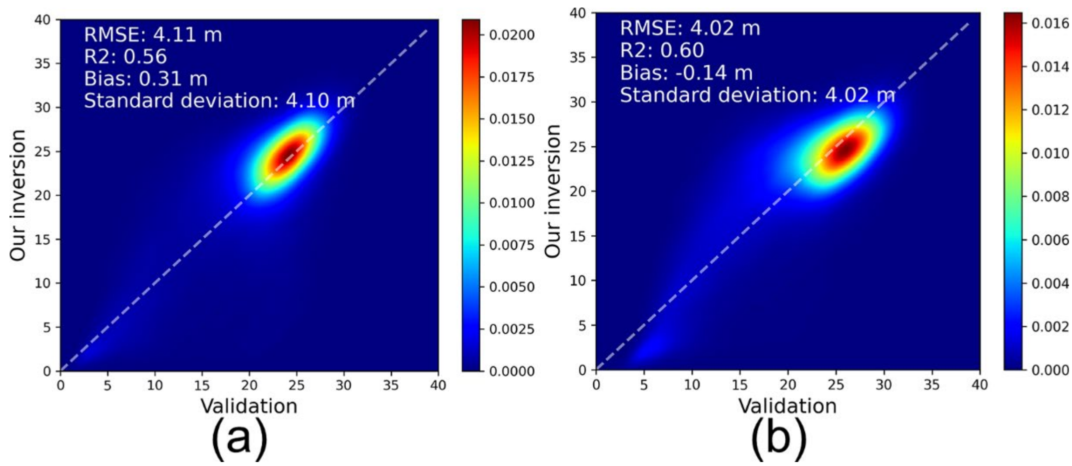

Figure 23: Density scatterplot of forest height comparison over the Harvard Forest site: (a) ALOS-1 mosaic versus LVIS LiDAR, and (b) ALOS-2 single scene versus LVIS LiDAR.

https://doi.org/10.5194/essd-2024-596
Preprint. Discussion started: 14 January 2025

4.2.3 White Mountain National Forest site

The evaluation of the forest height inversion approach should also be extended to mountainous areas like the WMNF site, considering the potential challenges GEDI and InSAR observations might face in these regions. These challenges include GEDI's geolocation shifts and slope effects, as well as radar's viewing geometry problems (e.g., layover, shadow, foreshortening).

As reference data, a high-resolution Canopy Height Model (CHM) was generated using small footprint GRANIT LiDAR data. As detailed in Section 3.2, due to the footprint difference between small footprint LiDAR data and GEDI observations, an equivalent RH metric must be extracted within the same footprint size as GEDI observations to ensure a fair comparison (see Figure 24 (a)). Without this adjustment, significant bias occurs if the GEDI-based forest height inversion is directly compared against the re-projected high-resolution CHM model simply by resampling or multi-pixel averaging. illustrates the difference between the ERH98 metric and the mean value (or ERH50 metric) in subfigure (a) and shows the maps of these two metrics in subfigures (b) and (c). It is evident that the ALOS-1-based forest height estimates, as shown in subfigure (d), are consistent with the ERH98 metric in subfigure (b). The differential height map and the density scatterplot are shown in Figure 25.

https://doi.org/10.5194/essd-2024-596
Preprint. Discussion started: 14 January 2025

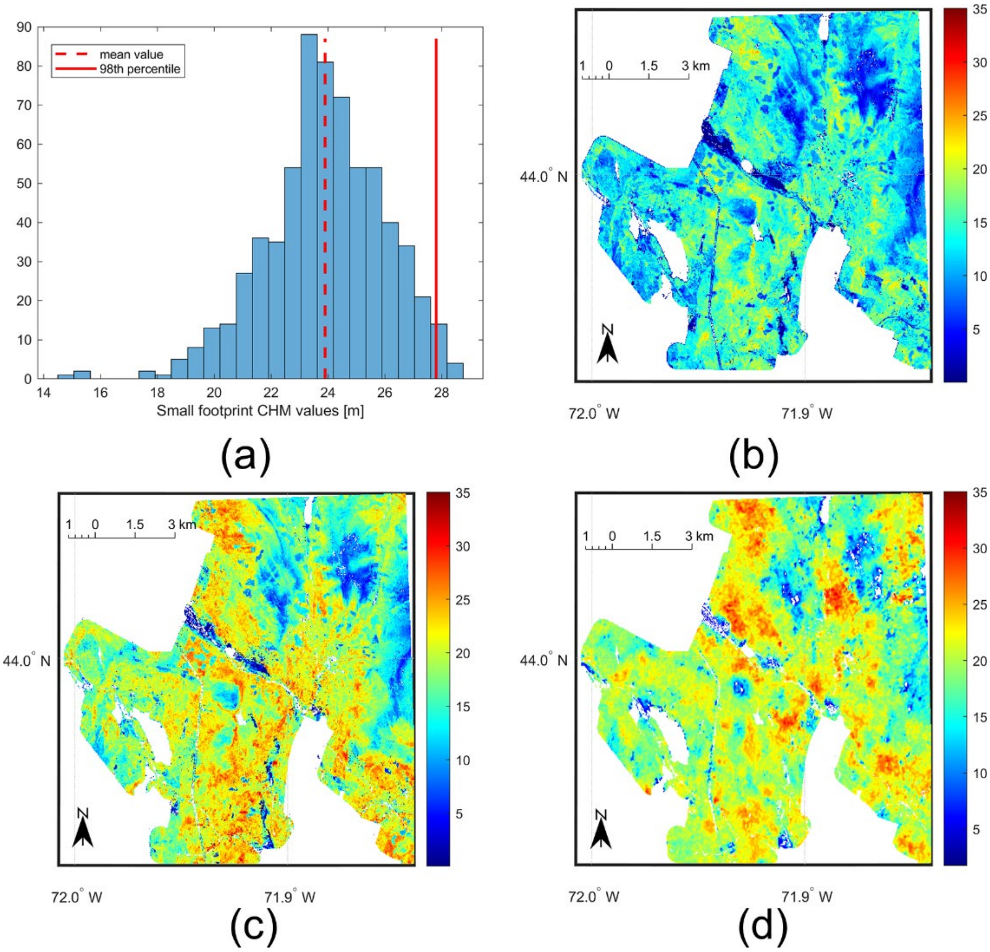

665 **Figure 24: (a) An example of histogram formed by small footprint CHM values within the GEDI footprint, with mean height and a 98-th percentile height marked by the red dashed and red solid lines, respectively. (b) 30 m gridded reprocessed forest height based on the ERH50 metric, (c) 30 m gridded reprocessed forest height based on the ERH98 metric and (d) corresponding forest height estimates extracted from ALOS-1 mosaic.**

https://doi.org/10.5194/essd-2024-596
Preprint. Discussion started: 14 January 2025

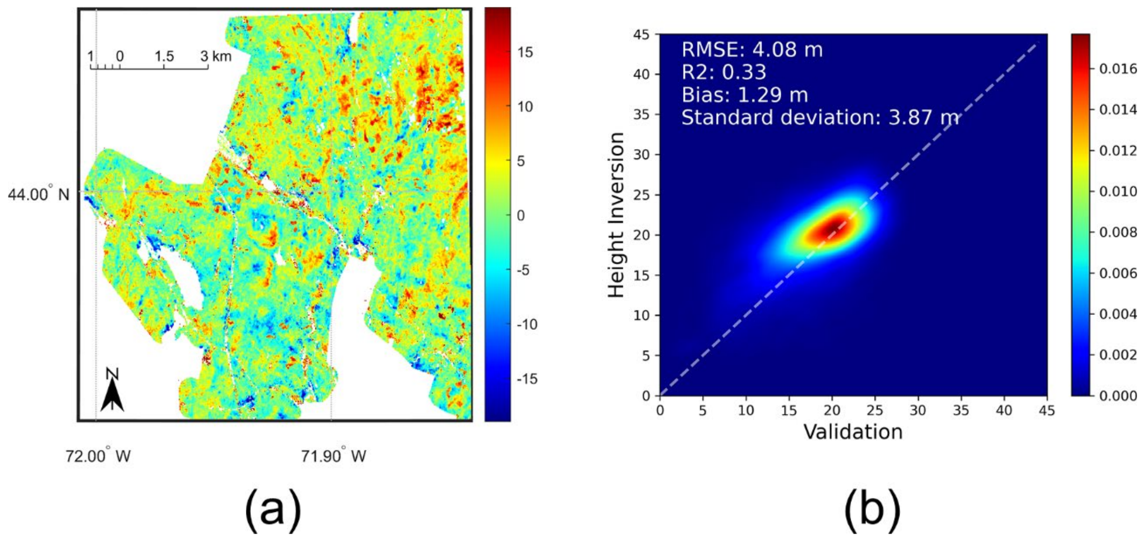

Figure 25: (a) Differential height map between the ALOS-1 mosaic and GRANIT ERH98 map and (b) the corresponding density scatterplots.

4.2.4 Summary of the validation results over the northeastern U.S.

Table 4 summarizes the error metrics of the forest height estimates (from either the ALOS-1 mosaic or the ALOS-2 single scene inversion when suitable InSAR pairs are available) across all the test sites in the New England Region considered in this study. The density scatterplots of all comparisons are depicted in Figure 26.

In summary, the proposed inversion approach is capable of estimating forest height with an RMSE of 3-4 m in areas such as Howland and Harvard Forests, characterized by relatively flat topography and minimal human activity influence. As a comparison, in hilly or suburban areas like WMNF, GMNF, and Naugatuck State Forest sites, an accuracy of 4-5 m is achieved. The ALOS-2 based inversion generally presents superior performance due to enhanced InSAR correlation behavior resulting from shorter temporal baselines, and less time discrepancy between radar and LiDAR data. For ALOS-1 inversion, the time mismatch between ALOS-1 and GEDI data is not a fatal problem as the inversion is carried out for temperate regions where the intact forest landscape and forest height (of mature forests) remain stable. Our two-fold solution for address forest change might not be perfect and introduce errors. However, besides these uncertainties, the forest height is estimated with an RMSE of 3–4 m/ha, suggesting that this part of error is relatively minor. This is also supported by the finding that the ALOS-1 based inversion is occasionally more accurate than ALOS-2 based estimates.

https://doi.org/10.5194/essd-2024-596
Preprint. Discussion started: 14 January 2025

Table 4 Error metrics for forest height inversion based on ALOS-1 or ALOS-2 InSAR data, compared with airborne LiDAR data across all forest sites in the New England region, at a 0.81-hectare aggregated pixel size. A dash ('-') indicates that no suitable ALOS-2 InSAR pairs.

Validation sites		ALOS-1 based	ALOS-2 based
Howland Forest	RMSE	3.81	3.59
	R2	0.47	0.51
	Bias	-0.34	0.02
	Standard Deviation	3.78	3.59
Harvard Forest	RMSE	4.11	4.02
	R2	0.56	0.6
	Bias	0.31	0.14
	Standard Deviation	4.10	4.02
White Mountain National Forest	RMSE	4.08	-
	R2	0.33	
	Bias	1.29	
	Standard Deviation	3.87	
Green Mountain National Forest	RMSE	4.97	-
	R2	0.53	
	Bias	0.46	
	Standard Deviation	4.95	
Naugatuck State Forest	RMSE	5.06	-
	R2	0.47	
	Bias	-0.84	
	Standard Deviation	5.01	

https://doi.org/10.5194/essd-2024-596
Preprint. Discussion started: 14 January 2025

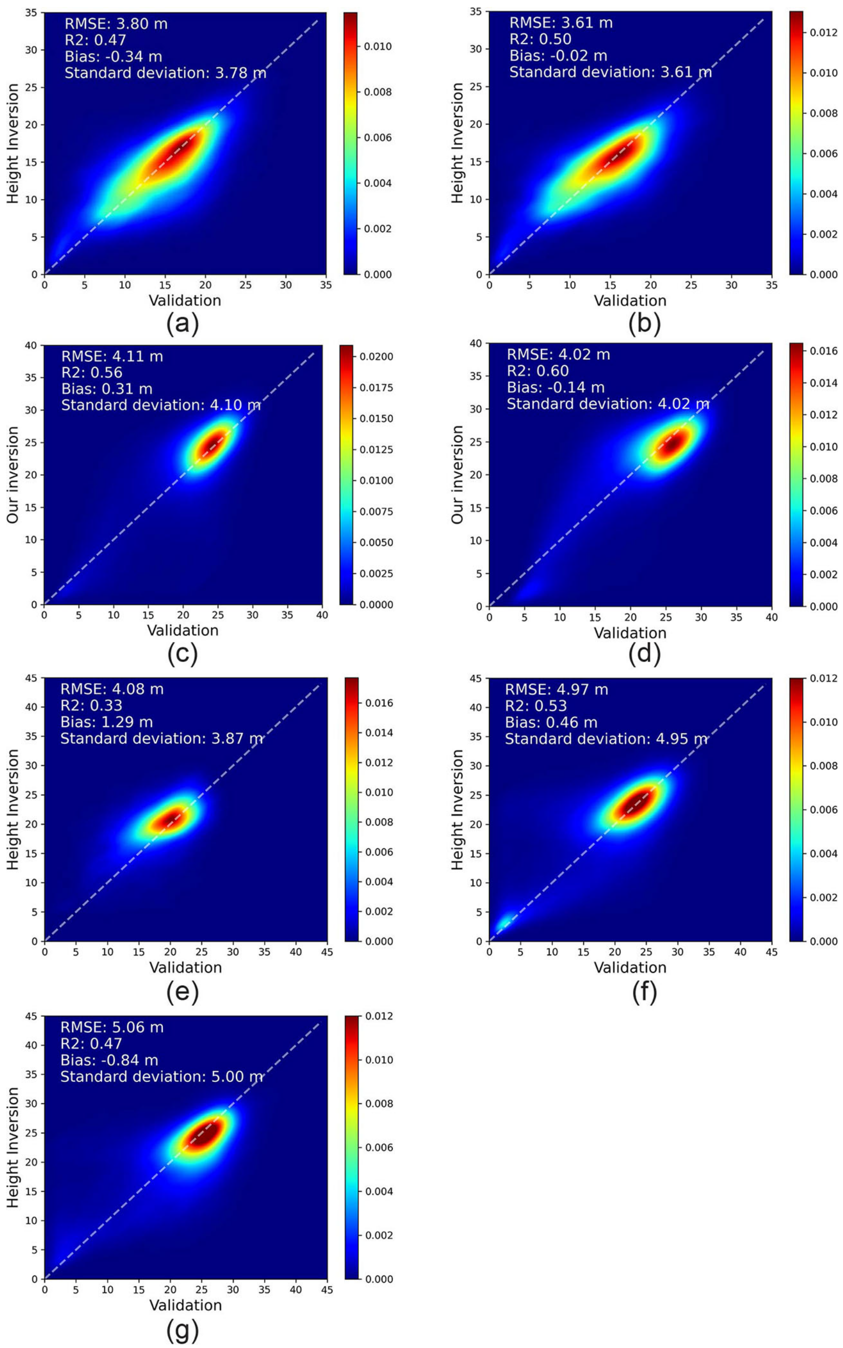

Figure 26: Density scatterplots comparing LiDAR validation data with forest height inversion estimates: (a) ALOS-1 and (b) ALOS-2 for the Howland Forest site, (c) ALOS-1 and (d) ALOS-2 for the Harvard Forests, and ALOS-1 estimates for (e) WMNF, (f) GMNF, and (g) Naugatuck State Forest.

https://doi.org/10.5194/essd-2024-596
Preprint. Discussion started: 14 January 2025

4.3 Validation against ALS data over the northeastern region of China

The forest height mosaic over the northeastern China was validated solely against small footprint ALS data at represenative forest sites. These high-resolution ALS data were processed into ERH98 metric maps based on the method as defined in Section 4.2.3. Similarly, two case studies over Hubao National Park and Genhe Forest Bureau are presented for detailed analysis. These two forest sites were chosen due to the significant dynamic range of tree height observed in both regions.

4.3.1 Hubao National Park Forest site

Hubao National Park is selected here as it represents one of the typical temperate regions with the richest biodiversity in terms of wildlife and plants in the northern hemisphere. The validation of forest height is shown in Figure 27: (a) is generated by reprocessing 1 m resolution CHM map acquired in 2018 into the ERH98 map using a window with the same size as GEDI footprint. Compared to the reference data, Figure 28 (b) and (c) show the forest height estimates based on ALOS-1 single scene (frame: 860, orbit: 421) inversion and based on a single pair of ALOS-2 data (frame: 860, orbit: 130). It can be observed from the density scatterplots in Figure 28 that both ALOS-1 mosaic and ALOS-2 single-scene based inversion results align well with the ALS ERH98 at an accuracy of 3.5-3.8 m with a R^2 up to 0.7. This yields accurate estimates comparable to airborne LiDAR measurements for both short and tall vegetation. Slightly better performance for ALOS-1 based inversion is attributed to the fact that the ALOS-1 InSAR data archive offers the possibility to pick out the best InSAR pair with better correlation behavior; however, the availability of proper ALOS-2 InSAR data is limited.

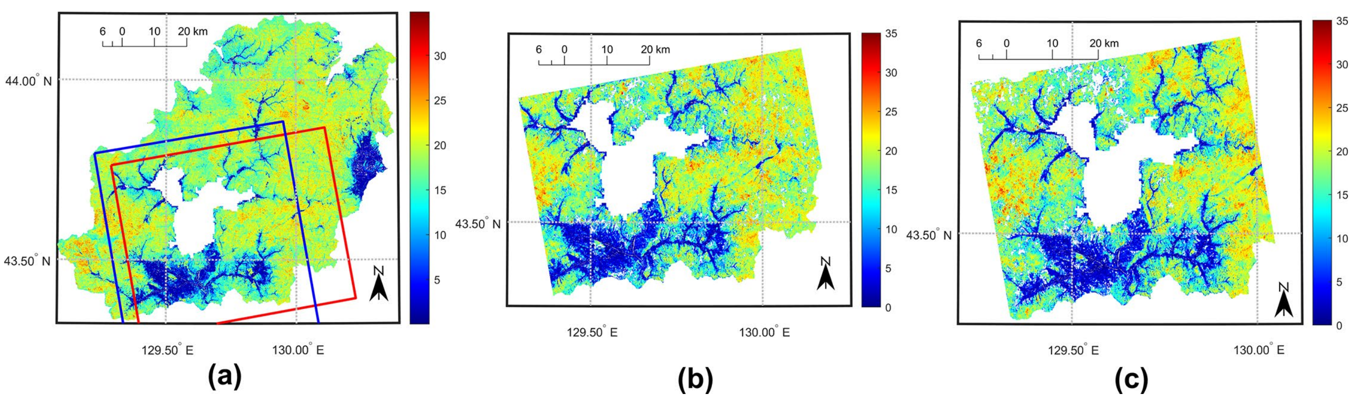

Figure 27: Comparison of the forest height inversion with LiDAR validation data at the Hubao National Park site: (a) ALS ERH98 metric map. The red rectangle denotes the coverage of (b) ALOS-1 based single-scene inversion, whereas the blue rectangle indicates the coverage of (c) ALOS-2 based single-scene inversion.

https://doi.org/10.5194/essd-2024-596
Preprint. Discussion started: 14 January 2025

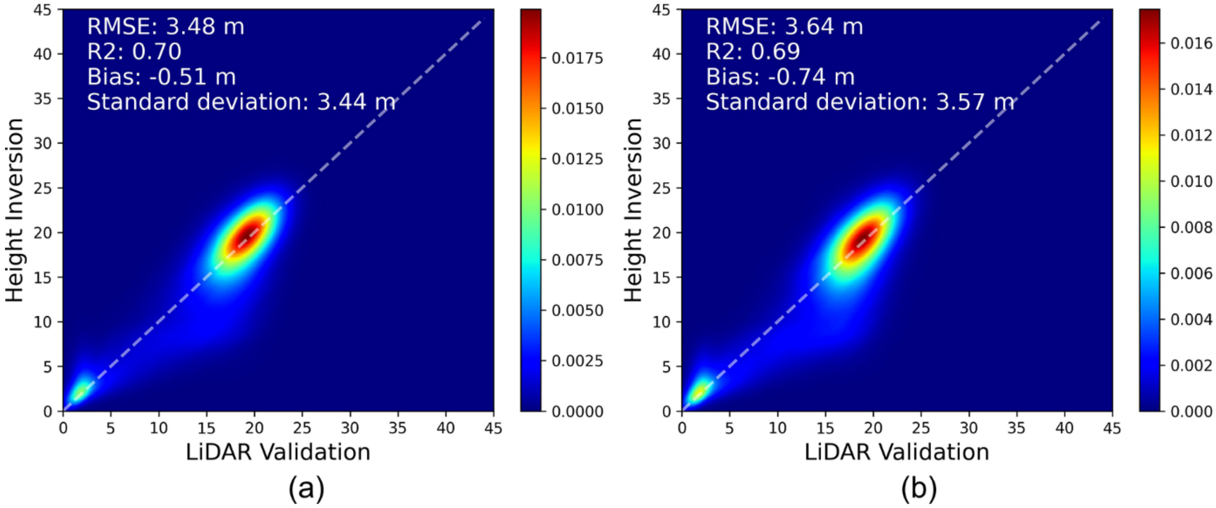

Figure 28: Density scatterplots comparing forest height inversion over the validation site in Hubao National Park: (a) ALOS-1 single scene versus ALS ERH98, and (b) ALOS-2 single scene versus ALS ERH98

4.3.2 Genhe Forest Bureau

Another case study in the northeast of China is the Genhe Forest Bureau, one of the northernmost places in China. Figure 29 exhibits (a) the reference ERH98 map regenerated from 1 m footprint airborne LiDAR data, (b) the corresponding forest height estimates extracted from the ALOS-1 forest height mosaic, and (c) the estimates from ALOS-2 single-scene inversion. It is evident in Figure 29 (a) that the spatial distribution of forest height is nearly identical in both the reference map and the inversion results. Furthermore, the inverted forest height closely aligns with the reference data, achieving an RMSE of 3.6 m and an R^2 of 0.65 (see Figure 30), thereby demonstrating the effectiveness and promising accuracy of this approach in boreal regions.

https://doi.org/10.5194/essd-2024-596
Preprint. Discussion started: 14 January 2025

Open Access Earth System Science Data Discussions

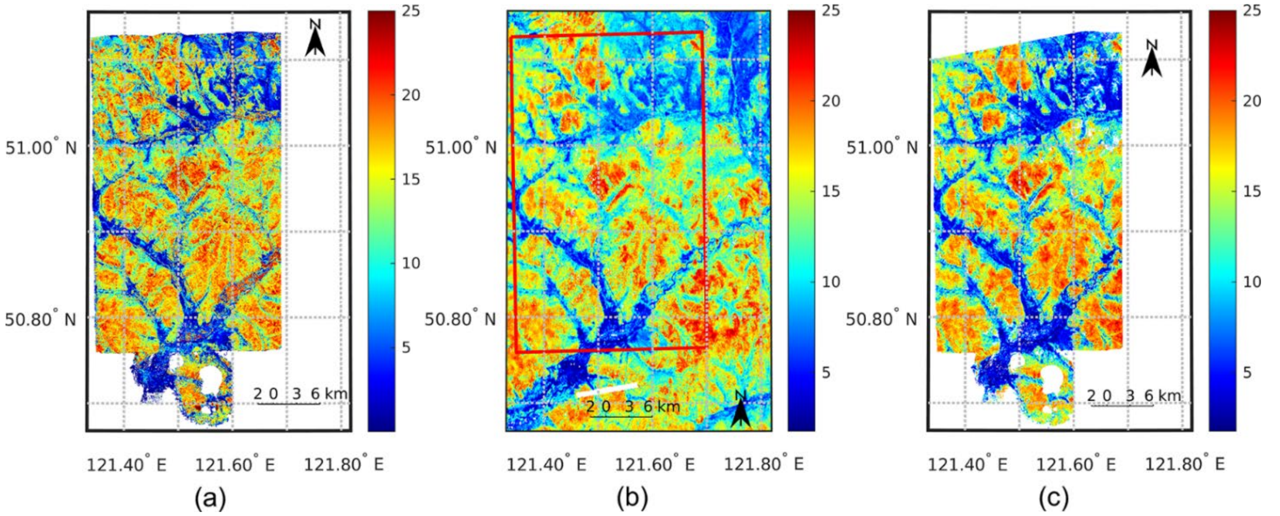

Figure 29: Comparison of the forest height inversion over the Genhe Forest Bureau: (a) ALS ERH98 metric generated based on 25 m footprint; (b) ALOS-1 mosaic with red rectangle box indicating the overlapping area with (a), and (c) ALOS-2 based single-scene inversion.

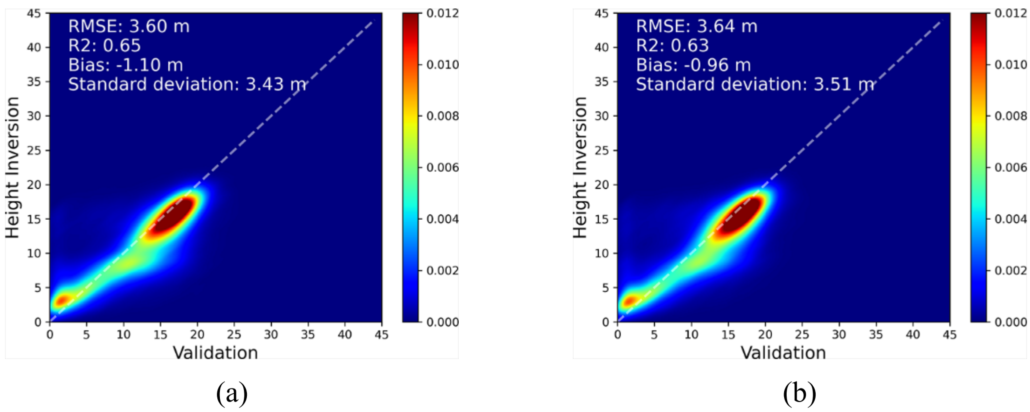

Figure 30: Density scatterplots of the comparison of forest height inversion over the Genhe Forest Bureau in Inner Mongolia province: (a) ALOS-1 mosaic versus ALS ERH98, and (b) ALOS-2 single scene versus ALS ERH98.

https://doi.org/10.5194/essd-2024-596
Preprint. Discussion started: 14 January 2025

4.3.3 Summary of the validation over the northeast of China

The forest height estimates of all the forest validation sites were compared against the ERH98 data generated from the small footprint airborne LiDAR data. The error metrics of all the comparisons (See Figure 31) are concluded in the Table 5. It can be observed that the best inversion performance is achieved at the site of Mengjiagang forest with an RMSE of 3.32 m and a R^2 up to 0.84. Most of forest height inversions present the negative bias, which may be attributed to the relatively weaker penetration capabilities for GEDI compared to the airborne LiDAR. Slightly less accurate estimates are provided by the ALOS-2 based inversion at the Saihanba forest site, attributed to the limited overlapping area between the ALOS-2 single-scene inversion and ALS validation observations. This limitation arises from the distribution of heterogeneous land covers influenced by human activities. In summary, almost all forest height estimates align well with the ERH98 ALS data, achieving an accuracy of 3-4 m (even below 3.5 m in three sites) with R^2 mostly above 0.65. This shows better inversion performance in areas farther away from the GEDI calibration sites in the northeastern U.S., due to the less forest disturbance activities in northeastern China (See Figure 13) compared to the northeastern U.S. as presented in Figure 14. In this way, the errors caused by the proposed two-folded solution for accounting for forest change are minimized.

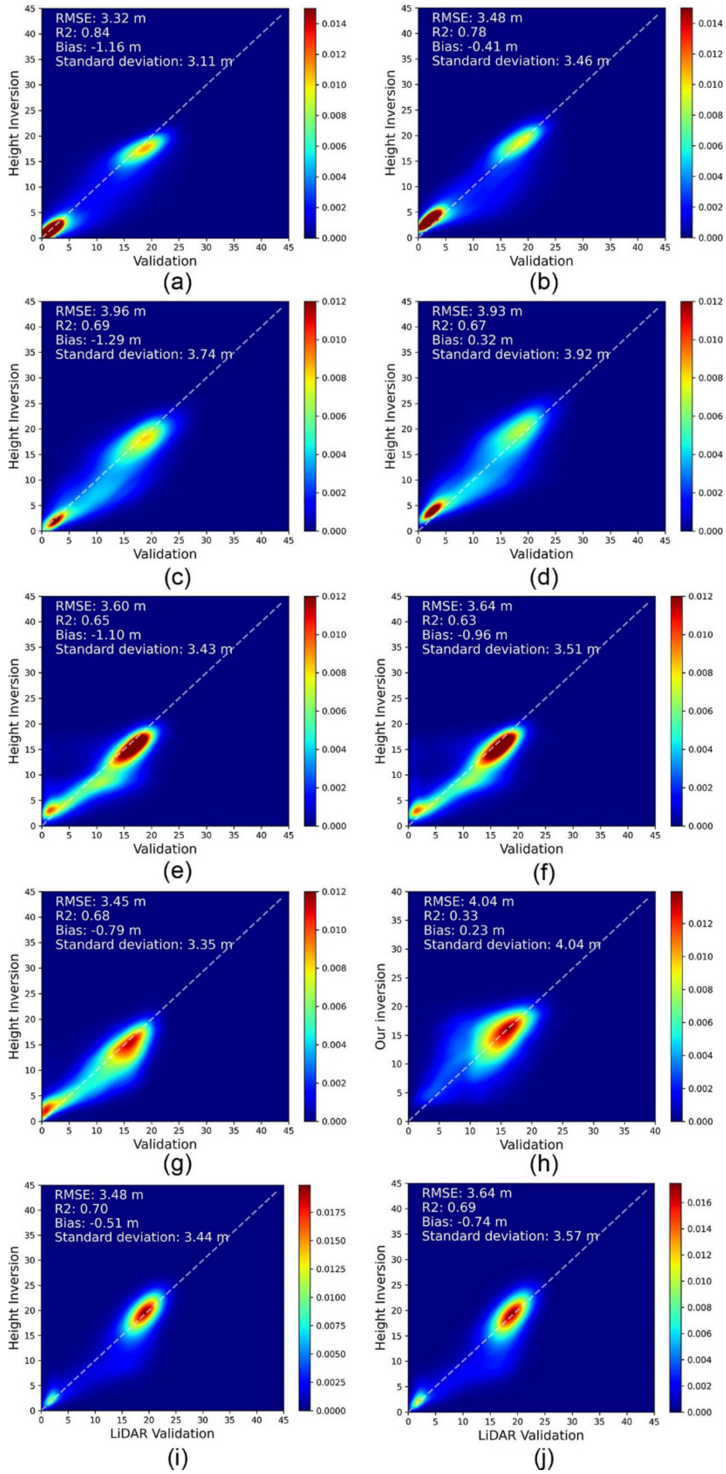

Figure 31: Density scatterplots of forest height inversions based on the ALOS-1 InSAR observations (left column), and the ALOS-2 observations (right column) for the forest sites (one site per row) listed in the same order as in Table 5.

https://doi.org/10.5194/essd-2024-596
Preprint. Discussion started: 14 January 2025

Table 5 Error metrics of forest height inversion (based on ALOS-1 and ALOS-2 data) against airborne LiDAR data in all the forest sites of the northeastern China at 0.81-hectare aggregated pixel size.

Validation sites		ALOS-1 based	ALOS-2 based
Mengjiagang Forest	RMSE	3.32	3.48
	R^2	0.84	0.78
	Bias	-1.16	-0.41
	Standard Deviation	3.11	3.46
Dagujia Forest	RMSE	3.96	3.93
	R^2	0.69	0.67
	Bias	-1.29	0.32
	Standard Deviation	3.74	3.92
Genhe Forest Bureau	RMSE	3.60	3.64
	R^2	0.65	0.63
	Bias	-1.1	-0.96
	Standard Deviation	3.43	3.51
Saihanba Forest	RMSE	3.45	4.04
	R^2	0.68	0.33
	Bias	-0.79	0.23
	Standard Deviation	3.35	4.04
Hubao National Park	RMSE	3.48	3.64
	R^2	0.7	0.69
	Bias	-0.51	-0.74
	Standard Deviation	3.44	3.57

5 Conclusions

This paper presented a global-to-local two-stage forest height inversion approach for large-scale forest stand height mapping using L-band spaceborne repeat-pass InSAR and spaceborne GEDI LiDAR. This work extended our previous efforts in forest stand height mapping (FSH: https://github.com/leiyangleon/FSH; Lei and Siqueira, 2014, Lei and Siqueira, 2015, Lei et al., 2018) at large scale by incorporating GEDI LiDAR samples for capturing local information. The sparsely yet extensively distributed LiDAR samples provided by the GEDI mission are used to parameterize the semi-empirical InSAR scattering model and to obtain forest height estimates. Building on earlier works (Lei et al., 2018; Lei and Siqueira, 2022), this paper removed the assumptions made imposed by the limited availability of calibration samples before, and developed a new inversion approach based on a global-to-local two-stage inversion scheme. An effective use of regional GEDI samples in this approach allows for finer characterization of temporal decorrelation patterns and thus higher accuracy in forest height inversion while also suppressing problems in individual GEDI sample, e.g. geolocation error. This approach was supported by fusing the ALOS-2 InSAR data and GEDI data under nearly concurrent condition. This approach is further applied to open-access ALOS-1 data for testing its mapping capabilities at large scale. To address the temporal mismatch between ALOS-1 data and GEDI data, the introduction of fusing ALOS-2 backscatter data and GEDI data is able to detect disturbed forest areas. Furthermore, a modified signal model is derived for addressing natural forest growth over temporate forest regions where the intact forest landscape and forest height are stable with slight change. Without forest growth data, this modified model is well approximated with original model via local fitting. For evaulating its performance, two forest height mosaic maps were generated to investigate the northeastern regions in the U.S. and China, covering a total area of 18 million hectares and 152 million hectares, respectively. Validation of the forest height estimates demonstrates substantial accuracy improvements achieved by the proposed approach compared to the previous efforts, i.e., from 4 m RMSE for 6.25-hectare aggregated pixel size to 3.8 m RMSE for 0.81-hectare aggregated pixel size at the Howland Forest site. The proposed fusion approach not only addresses the sparse spatial sampling problem of the GEDI mission, but also improves the accuracy of forest height estimates compared to the GEDI interpolated height estimates by 20%. The extensive evaluation of forest height inversion against LVIS LiDAR data over northeastern U.S. indicates an accuracy of 3-4 m on the order of 0.81 hectare over smooth areas and 4-5 m over hilly areas, while the forest height estimates over northeastern China compare well with small footprint LiDAR validation data even at an accuracy of below 3.5 m on the order of sub-hectare and with R^2 mostly above 0.6.

The current limitations of this work include the complicated InSAR correlation behavior induced by weather condition changes (e.g., precipitation) when only limited InSAR pairs are available. This issue can be addressed with future InSAR missions where InSAR data stacks quickly accumulate within each season, allowing for a synthetic seasonal InSAR coherence map to be generated by averaging or taking the maximum value of all available InSAR pairs (Kellndorfer et al., 2022). For example, given the 12-day repeat cycle of NISAR, there would be 7 (or 30) 12-day InSAR pairs during each season (or year), enabling the synthesis of seasonally (or annually) averaged InSAR coherence observations for more robust height inversion.

As for the temporal mismatch between ALOS-1 and GEDI data, the two-fold solution is provided for adressing the forest changes. This solution might not be perfect for addressing the complex temporal evolution of forests. Provided that the achieved forest estimation accuracy at 3-4 m/ha, this should not be a fatal problem over the temporate forest regions where intact forest landscape and forest height remain alomst stable, and only change slightly as trees grow.

https://doi.org/10.5194/essd-2024-596
Preprint. Discussion started: 14 January 2025

Additionally, this approach reies on accurate and well-distributed calibration samples provided by GEDI observations. Such requirements may not always be met due to: 1) slopes causing biased forest height estimates for GEDI, and 2) limited observation capabilities over the boreal zone, along with reduced sample collection over tropical regions near the equator. The first issue can be mitigated by using the RH metric extracted from slope-corrected waveforms (Wang et al., 2019). The latter problem may be addressed by incorporating forest height measurements from other LiDAR satellites, such as NASA's ICESat-1/2. Forest height mapping based on the proposed approach can be improved (and also easily adapted) by fusing ALOS-1 with both GEDI and ICESat-1/2 data, particularly for tropical regions.

Despite these limitations, the achieved accuracy of forest height inversion at a sub-hectare pixel size using the proposed approach with publicly available spaceborne InSAR and LiDAR datasets presents promising values in the context of existing and future spaceborne InSAR missions (e.g., JAXA's ALOS/ALOS-2/ALOS-4, NASA-ISRO's NISAR, and China's LuTan-1) and LiDAR missions (e.g., JAXA's MOLI, NASA's GEDI, and China's TECIS). It may serve as a cost-effective complementary alternative for large-scale forest height investigation when spaceborne bistatic InSAR (for applying PolInSAR and/or TomoSAR) data are unavailable.

6 Data availability

The forest height mosaics over the northeastern parts of U.S. and China are available at https://doi.org/10.5281/zenodo.11640299 (Yu and Lei, 2024). The used ALOS-1 data can be found via the Alaska Satellite Facility at https://search.asf.alaska.edu/#/?dataset=ALOS. GEDI data (from 2018 to 2023) can be downloaded from the EARTHDATA SEARCH website at https://search.earthdata.nasa.gov/. Regarding the validation data, the LVIS and GRANIT LiDAR data can be found at https://lvis.gsfc.nasa.gov/Data/Maps/GEDI2021Map.html and https://lidar.unh.edu/map/. Lei and Siqueira, 2022

7 Software Tools

The forest height mosaics are generated using the following software tools. First, ISCE with Version 2.4+ (https://github.com/isce-framework/isce2/releases; in particular the "stripmapApp" function) is used to preprocess the two ALOS-1/-2 images for procduing geocoded interferomteric coherence maps. Then, *FSH* Software Version 2 (https://github.com/Yanghai717/FSHv2) is used to invert and forest height by fusing GEDI and InSAR data and perform the mosaicking. Several preprocessing steps utilize basic Python libraries from FSH Version 1: https://github.com/leiyangleon/FSH.

https://doi.org/10.5194/essd-2024-596
Preprint. Discussion started: 14 January 2025

Acknowledgement

This study was sponsored by the National Key R&D Program of China (2022YFB3903300 and 2022YFB3903301) and the National Natural Science Foundation of China (Grant No. 62301529). The author would also like to thank the Japan Aerospace Exploration Agency for providing ALOS-1 and ALOS-2 data, and the National Aeronautics and Space Administration for providing GEDI data.

Author contributions. YL, PS, JC designed the study. YY, YL developed the processing software (*FSH v2*), YY,YL designed calibration/valalition tests and YY XL, DG, AF,YP, WH carried out the validation tests. YY prepared the manuscript with contributions from all co-authors.

Competing interests. Authors declare that they have no conflict of interest.

References

Abdalati, W., Zwally, H. J., Bindschadler, R., Csatho, B., Farrell, S. L., Fricker, H. A., Harding, D., Kwok, R., Lefsky, M., and Markus, T.: The ICESat-2 laser altimetry mission, Proceedings of the IEEE, 98, 735-751, 2010.

Ahmed, R., Siqueira, P., Hensley, S., Chapman, B., and Bergen, K.: A survey of temporal decorrelation from spaceborne L-Band repeat-pass InSAR, Remote Sensing of Environment, 115, 2887-2896, 2011.

Angelsen, A.: Realising REDD+: National strategy and policy options, Cifor2009.

Askne, J. I., Fransson, J. E., Santoro, M., Soja, M. J., and Ulander, L. M.: Model-based biomass estimation of a hemi-boreal forest from multitemporal TanDEM-X acquisitions, Remote Sensing, 5, 5574-5597, 2013.

Askne, J. I. H., Dammert, P. B. G., Ulander, L. M. H., and Smith, G.: C-band repeat-pass interferometric SAR observations of the forest, IEEE Transactions on Geoscience and Remote Sensing, 35, 25-35, 1997.

Bamler, R. and Hartl, P.: Synthetic aperture radar interferometry, Inverse problems, 14, R1, 1998.

Choi, C., Cazcarra-Bes, V., Guliaev, R., Pardini, M., Papathanassiou, K. P., Qi, W., Armston, J., and Dubayah, R. O.: Large-scale forest height mapping by combining TanDEM-X and GEDI data, IEEE Journal of Selected Topics in Applied Earth Observations and Remote Sensing, 16, 2374-2385, 2023.

Deledalle, C.-A., Denis, L., Tupin, F., Reigber, A., and Jäger, M.: NL-SAR: A unified nonlocal framework for resolution-preserving (Pol)(In) SAR denoising, IEEE Transactions on Geoscience and Remote Sensing, 53, 2021-2038, 2014.

Dubayah, R., Blair, J. B., Goetz, S., Fatoyinbo, L., Hansen, M., Healey, S., Hofton, M., Hurtt, G., Kellner, J., and Luthcke, S.: The Global Ecosystem Dynamics Investigation: High-resolution laser ranging of the Earth's forests and topography, Science of remote sensing, 1, 100002, 2020.

Fayad, I., Baghdadi, N., and Lahssini, K.: An assessment of the GEDI lasers' capabilities in detecting canopy tops and their penetration in a densely vegetated, tropical area, Remote Sensing, 14, 2969, 2022.

Gatelli, F., Guamieri, A. M., Parizzi, F., Pasquali, P., Prati, C., and Rocca, F.: The wavenumber shift in SAR interferometry, IEEE Transactions on Geoscience and Remote Sensing, 32, 855-865, 1994.

Hansen, M. C., Potapov, P. V., Moore, R., Hancher, M., Turubanova, S. A., Tyukavina, A., Thau, D., Stehman, S. V., Goetz, S. J., and Loveland, T. R.: High-resolution global maps of 21st-century forest cover change, science, 342, 850-853, 2013.

Hofton, M., Blair, J. B., Story, S., and Yi, D.: Algorithm Theoretical Basis Document (ATBD), Washington, DC, USA: NASA, 2020.

Kellndorfer, J., Cartus, O., Lavalle, M., Magnard, C., Milillo, P., Oveisgharan, S., Osmanoglu, B., Rosen, P. A., and Wegmüller, U.: Global seasonal Sentinel-1 interferometric coherence and backscatter data set, Scientific Data, 9, 73, 10.1038/s41597-022-01189-6, 2022.

Kellogg, K., Hoffman, P., Standley, S., Shaffer, S., Rosen, P., Edelstein, W., Dunn, C., Baker, C., Barela, P., and Shen, Y.: NASA-ISRO synthetic aperture radar (NISAR) mission, 2020 IEEE Aerospace Conference, 1-21,

Krieger, G., Moreira, A., Fiedler, H., Hajnsek, I., Werner, M., Younis, M., and Zink, M.: TanDEM-X: A satellite formation for high-resolution SAR interferometry, IEEE Transactions on Geoscience and Remote Sensing, 45, 3317-3341, 2007.

Lavalle, M., Simard, M., and Hensley, S.: A Temporal Decorrelation Model for Polarimetric Radar Interferometers, IEEE Transactions on Geoscience and Remote Sensing, 50, 2880-2888, 10.1109/TGRS.2011.2174367, 2012.

Lei, Y.: Electromagnetic scattering models for InSAR correlation measurements of vegetation and snow, 2016.

Lei, Y. and Siqueira, P.: Estimation of forest height using spaceborne repeat-pass L-band InSAR correlation magnitude over the US state of Maine, Remote Sensing, 6, 10252-10285, 2014.

Lei, Y. and Siqueira, P.: Refined forest stand height inversion approach with spaceborne repeat-pass l-band sar interferometry and gedi lidar data, IGARSS 2022-2022 IEEE International Geoscience and Remote Sensing Symposium, 6388-6391,

Lei, Y., Lucas, R., Siqueira, P., Schmidt, M., and Treuhaft, R.: Detection of forest disturbance with spaceborne repeat-pass SAR interferometry, IEEE Transactions on Geoscience and Remote Sensing, 56, 2424-2439, 2017.

Lei, Y., Siqueira, P., Torbick, N., Ducey, M., Chowdhury, D., and Salas, W.: Generation of large-scale moderate-resolution forest height mosaic with spaceborne repeat-pass SAR interferometry and lidar, IEEE Transactions on Geoscience and Remote Sensing, 57, 770-787, 2018.

Loveland, T. R. and Dwyer, J. L.: Landsat: Building a strong future, Remote Sensing of Environment, 122, 22-29, https://doi.org/10.1016/j.rse.2011.09.022, 2012.

https://doi.org/10.5194/essd-2024-596
Preprint. Discussion started: 14 January 2025

Lucas, R. M., Cronin, N., Lee, A., Moghaddam, M., Witte, C., and Tickle, P.: Empirical relationships between AIRSAR backscatter and LiDAR-derived forest biomass, Queensland, Australia, Remote Sensing of Environment, 100, 407-425, 2006.

Masson-Delmotte, V., Zhai, P., Pirani, A., Connors, S. L., Péan, C., Berger, S., Caud, N., Chen, Y., Goldfarb, L., and Gomis, M.: Climate change 2021: the physical science basis, Contribution of working group I to the sixth assessment report of the intergovernmental panel on climate change, 2, 2391, 2021.

Monti-Guarnieri, A., Manzoni, M., Giudici, D., Recchia, A., and Tebaldini, S.: Vegetated target decorrelation in SAR and interferometry: models, simulation, and performance evaluation, Remote Sensing, 12, 2545, 2020.

Pan, Y., Birdsey, R. A., Fang, J., Houghton, R., Kauppi, P. E., Kurz, W. A., Phillips, O. L., Shvidenko, A., Lewis, S. L., and Canadell, J. G.: A large and persistent carbon sink in the world's forests, science, 333, 988-993, 2011.

Pang, Y., Li, Z., Ju, H., Lu, H., Jia, W., Si, L., Guo, Y., Liu, Q., Li, S., Liu, L., Xie, B., Tan, B., and Dian, Y.: LiCHy: The CAF's LiDAR, CCD and Hyperspectral Integrated Airborne Observation System, Remote Sensing, 8, 398, 2016.

Park, S. W., Linsen, L., Kreylos, O., Owens, J. D., and Hamann, B.: Discrete sibson interpolation, IEEE Transactions on visualization and computer graphics, 12, 243-253, 2006.

Potapov, P., Yaroshenko, A., Turubanova, S., Dubinin, M., Laestadius, L., Thies, C., Aksenov, D., Egorov, A., Yesipova, Y., and Glushkov, I.: Mapping the world's intact forest landscapes by remote sensing, Ecology and Society, 13, 2008.

Riofrío, J., White, J. C., Tompalski, P., Coops, N. C., and Wulder, M. A.: Modelling height growth of temperate mixedwood forests using an age-independent approach and multi-temporal airborne laser scanning data, Forest Ecology and Management, 543, 121137, https://doi.org/10.1016/j.foreco.2023.121137, 2023.

Rosen, P. A., Gurrola, E., Sacco, G. F., and Zebker, H.: The InSAR scientific computing environment, EUSAR 2012; 9th European conference on synthetic aperture radar, 730-733,

Rosenqvist, A., Shimada, M., Ito, N., and Watanabe, M.: ALOS PALSAR: A pathfinder mission for global-scale monitoring of the environment, IEEE Transactions on Geoscience and Remote Sensing, 45, 3307-3316, 2007.

Rosenqvist, A., Shimada, M., Suzuki, S., Ohgushi, F., Tadono, T., Watanabe, M., Tsuzuku, K., Watanabe, T., Kamijo, S., and Aoki, E.: Operational performance of the ALOS global systematic acquisition strategy and observation plans for ALOS-2 PALSAR-2, Remote Sensing of Environment, 155, 3-12, 2014.

Santoro, M., Cartus, O., Carvalhais, N., Rozendaal, D. M., Avitabile, V., Araza, A., De Bruin, S., Herold, M., Quegan, S., and Rodríguez-Veiga, P.: The global forest above-ground biomass pool for 2010 estimated from high-resolution satellite observations, Earth System Science Data, 13, 3927-3950, 2021.

Schutz, B. E., Zwally, H. J., Shuman, C. A., Hancock, D., and DiMarzio, J. P.: Overview of the ICESat mission, Geophysical research letters, 32, 2005.

Siqueira, P., Armston, J., Chapman, B., Christensen, A., Cushman, K., Das, A., Dubayah, R., Kellndorfer, J., McDonald, K., and Patnaik, C.: Ecosystem Science with NISAR: Final Preparations in The Pre-Launch Period, IGARSS 2024-2024 IEEE International Geoscience and Remote Sensing Symposium, 6628-6630,

https://doi.org/10.5194/essd-2024-596
Preprint. Discussion started: 14 January 2025

Torres, R., Snoeij, P., Geudtner, D., Bibby, D., Davidson, M., Attema, E., Potin, P., Rommen, B., Floury, N., and Brown, M.: GMES Sentinel-1 mission, Remote sensing of environment, 120, 9-24, 2012.

Treuhaft, R. N. and Siqueira, P. R.: Vertical structure of vegetated land surfaces from interferometric and polarimetric radar, Radio science, 35, 141-177, 2000.

Yu, Y. and Saatchi, S.: Sensitivity of L-band SAR backscatter to aboveground biomass of global forests, Remote sensing, 8, 522, 2016.

Yu, Y., Balz, T., Luo, H., Liao, M., and Zhang, L.: GPU accelerated interferometric SAR processing for Sentinel-1 TOPS data, Computers and geosciences, 129, 12-25, 2019.

Yu, Y. and Lei, Y.: Large-scale Forest Stand Height mapping for the northeast of U.S. and China using L-band spaceborne repeat-pass InSAR and GEDI, Zenodo [data set], https://doi.org/10.5281/zenodo.11640299, 2024.

Zebker, H. A. and Villasenor, J.: Decorrelation in interferometric radar echoes, IEEE Transactions on geoscience and remote sensing, 30, 950-959, 1992.